



OPEN ACCESS

EDITED BY

Joel Roskin,
Bar-Ilan University, Israel

REVIEWED BY

Xiaodong Miao,
Linyi University, China
Giora Jehiel Kidron,
Hebrew University of Jerusalem, Israel

*CORRESPONDENCE

Shimrit Maman,
✉ tiroshs@bgu.ac.il

SPECIALTY SECTION

This article was submitted to Quaternary Science, Geomorphology and Paleoenvironment, a section of the journal Frontiers in Earth Science

RECEIVED 21 December 2022

ACCEPTED 17 March 2023

PUBLISHED 14 April 2023

CITATION

Petrović MZ, Blumberg DG, Orlovsky L and Maman S (2023), Spatiotemporal analysis of dune stabilization in the Kyzylkum and Karakum sandy deserts. *Front. Earth Sci.* 11:1129360. doi: 10.3389/feart.2023.1129360

COPYRIGHT

© 2023 Petrović, Blumberg, Orlovsky and Maman. This is an open-access article distributed under the terms of the [Creative Commons Attribution License \(CC BY\)](https://creativecommons.org/licenses/by/4.0/). The use, distribution or reproduction in other forums is permitted, provided the original author(s) and the copyright owner(s) are credited and that the original publication in this journal is cited, in accordance with accepted academic practice. No use, distribution or reproduction is permitted which does not comply with these terms.

Spatiotemporal analysis of dune stabilization in the Kyzylkum and Karakum sandy deserts

Marijana Z. Petrović¹, Dan G. Blumberg², Leah Orlovsky¹ and Shimrit Maman^{3*}

¹Jacob Blaustein Institutes for Desert Research, Ben-Gurion University of the Negev, Sede-Boker, Israel,

²The Department of Environmental, Geoinformatics and Urban Planning Sciences, Ben-Gurion University of the Negev, Beer-Sheva, Israel, ³Homeland Security Research Institute, Ben-Gurion University of the Negev, Beer-Sheva, Israel

Sand seas and dune bedforms are climatic chronicles that have a wide range of scientific meanings. The Karakum and Kyzylkum sand seas in Central Asia span ~500,000 km², among the largest sand seas on Earth; yet, very little is known about their emergence and stabilization. Further, the internationally accessible literature lacks comprehensive studies on the interactions between contemporary climate and dune morphodynamics for this region. In this study, we applied the conventional approach for examining wind data—Fryberger's drift equations and the latest Copernicus ERA5 wind reanalysis model—to demonstrate that the Karakum and Kyzylkum deserts had (and continue to have) low-energy environments during 1950–2019. Time-series multidimensional raster analysis and data mining indicated that 93% of surveyed desert areas were subjected to low-energy wind conditions during the last 70 years. The decrease in wind energy was further confirmed using the partitioning around medoids (PAM) unsupervised machine-learning clustering method and Getis-Ord Gi* statistics. Such an environmental setting promotes plant growth and biogenic crust development, and strengthens dune stability across the deserts. Furthermore, the results suggested that the spatial patterns of active dune morphologies (e.g., complex barchanoid ridges and overlaying superimpositions) were closely linked to the drift direction, power, and variability of contemporary winds, whereas stabilized aeolian formations (e.g., distinct formations of complex and compound vegetated linear dunes) indicated debatable disassociations. The relationship between the recognized orientation of the surveyed dune types and the computed resultant drift direction did not change significantly, suggesting that over time, the winds in these areas have most likely varied in strength, but not in direction. The calculated drift powers are not sufficient for the formation of registered mega profiles. Rather, they bolster dunes stability, stressing both deserts as indicative of earlier climatic eras that permitted aeolian sand activity and severe shifts that have initiated their steadiness. This is the first comprehensive study to statistically evaluate the links between the contemporary climate and dune morphologies of the Karakum and Kyzylkum deserts. Our study can serve as a foundation for future studies on climate change, dune mapping, and optically stimulated luminescence (OSL) dating, while offering a broad understanding of the region's paleo and contemporary environmental systems dynamics.

KEYWORDS

dune morphodynamics, climate, ERA5, Fryberger, time-series multidimensional raster analysis, machine learning clustering, paleo-climate

1 Introduction

Extending from the eastern Caspian Sea coast in Turkmenistan to the Syr-Darya River valley in Kazakhstan (Figure 1), the Karakum and Kyzylkum sand seas in Central Asia cover ~500,000 km². As most of the world's sand seas are located in low-topography environments (Wilson, 1973; Livingstone et al., 2010), the Karakum (black sands) and Kyzylkum (red sands) deserts occupies the Turan lowlands, and are crossed by the Amu-Darya River. When combined, the Karakum and Kyzylkum Central Asian deserts (hereinafter referred to as KKCAD) are one of the world's largest sand seas (Maman et al., 2021). Even though the arid Central Asian deserts provide an excellent natural laboratory for studying land surface processes and the interactions between different landforms and the atmosphere (Fitzsimmons et al., 2020), due to the vastness of the region, limited meteorological data and access to the field, there is a lack of detailed studies in the domain of paleo and current climatic performances and their interactions with dunes morphodynamics. In addition, the international scientific literature related to classifying and understanding the spatial attributes of the desert dune forms in KKCAD, with respect to wind power and directionality, is limited, in comparison to the studies on other globally recognized sand seas, such as Namib (e.g., Lancaster, 1983; Lancaster, 1989; Livingstone et al., 2010), Sahara (e.g., Breed et al., 1979; Hu et al., 2021), Kalahari (e.g., Ashkenazy et al., 2011; Tsoar, 2013), and Takla Makan (e.g., Breed et al., 1979; Wang et al., 2002).

The stability of the KKCAD was briefly discussed by Wilson (1973), Pye and Tsoar (1990), Lancaster (1995), and Thomas (1997), who classified the area as active, and by Babaev et al. (1994), Jumashov (1999), and Maman et al. (2011, 2021), who

categorized the region as stable. At present, most sand seas are partially vegetated, and frequently described as partially or entirely relict (Twidale, 1981; Pye and Tsoar, 2009), as it is the case with KKCAD. However, in arid dune locations that receive some rainfall, permanent flora may be expected, which adds to the complexity regarding the classification of dune stability (Pye and Tsoar, 2009; Kinast et al., 2013). According to Maman et al. (2011), biogenic crusts and psammophytic (sand-loving) plants retain the bulk of the dunes in the stable region, nearly 95% of the total desert land; thus, only 5% of the desert land is active. Based on the optically stimulated luminescence (OSL) dating of 21 interdunal-sand samples collected predominantly from the Kyzylkum Desert (Maman et al., 2021) the ages of the dunes most recent stabilization phase are dated to the Mid to Late Holocene period, ranging between 3 and 7 ka, for both sand seas, when the climate changed from cold and dry to warm and wet. The Mid-Holocene sand sea stabilization suggests a progressive temperature shift from the last glacial maximum (LGM) to the early Holocene, excluding the Tian Shan range that differs because it is impacted by Asian Monsoons (Xu et al., 2010). Based on the theory that dune-building events are associated with glacial aridity (Sarnthein, 1978) and/or increased windiness related to glacial and cold events (McGee et al., 2010; Roskin et al., 2011a; Roskin et al., 2011b), Maman et al. (2021) suggested that the Mid-Holocene transition, from dry and cold to more humid and warm conditions with low wind power, led to the changes in the current landscapes of the KKCAD. In summary, it is proposed that dune stability in the region was facilitated by enough precipitation and decreasing wind power in the Mid-Holocene, which were no longer sufficient to promote sand

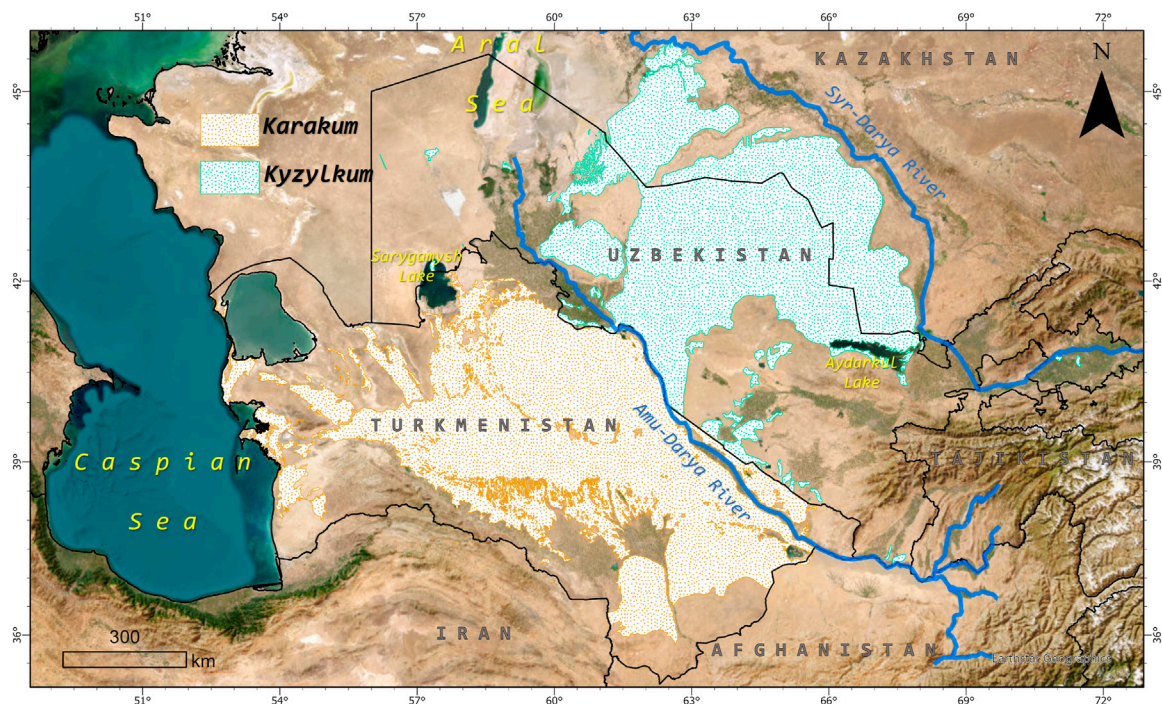
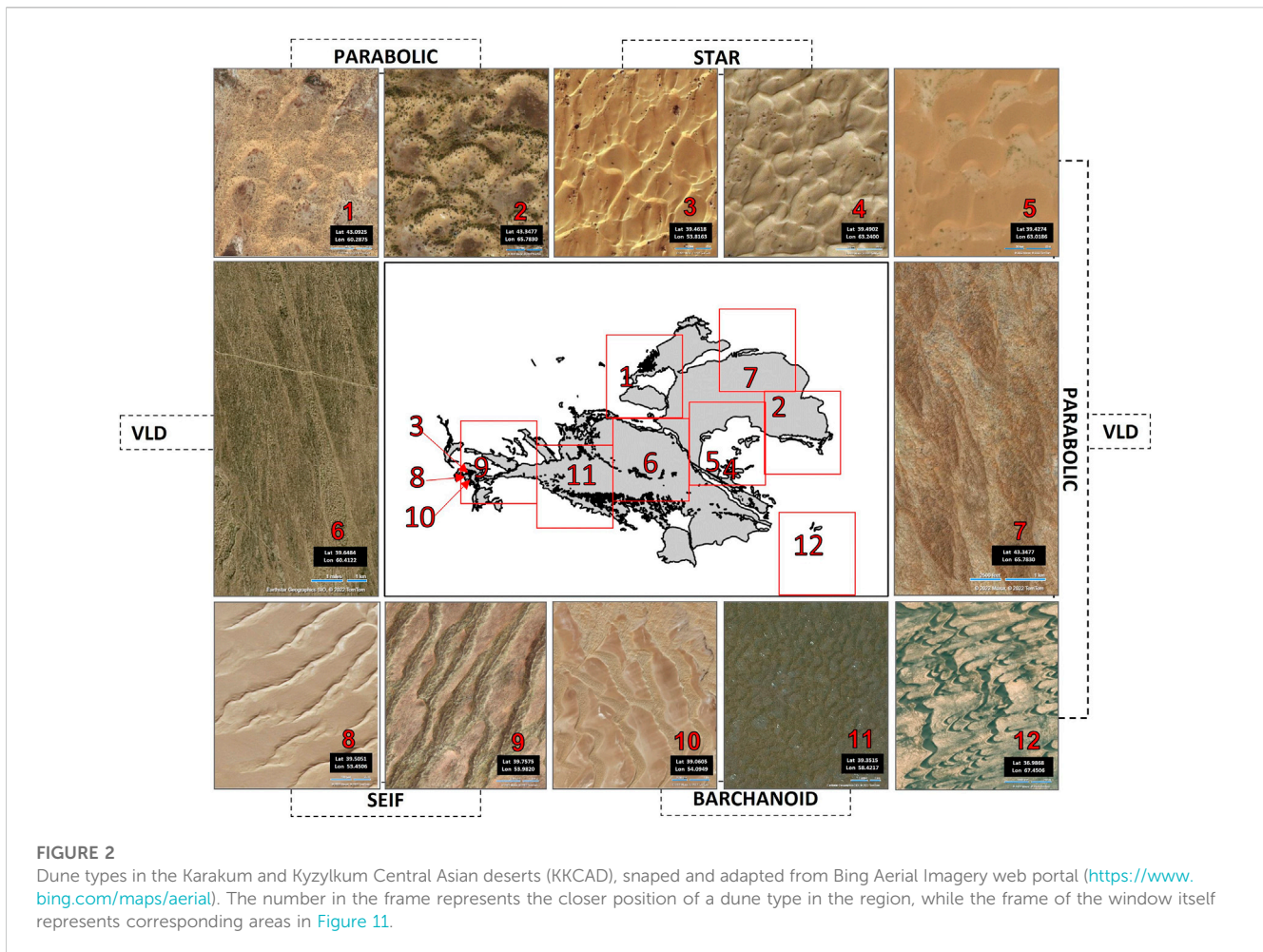


FIGURE 1
Map of the study area: location of Karakum and Kyzylkum Central Asian deserts, adapted from Maman et al. (2011).



movement or impede germination thus have led to dunes stabilization, which has continued to this day.

According to a basic review of the region’s aeolian formations (Maman et al., 2021), KCCAD depicts compound and complex relief where two or more dunes of the same or distinct kinds coexist or overly one another. VLDs are identified at all states of complexity and are by far the most frequent dune type in KCCAD (Maman et al., 2011; 2021). Some areas in the KCCAD region are completely stable, whereas others remain active, coexisting with a stable dune profile corresponding to the same climatic and geographical environment (Maman et al., 2011), indicating a separate time of mobilization. Notably, in the current literature, there are no studies on the genesis or evolution of the aeolian structures in both deserts. Furthermore, for this region, there are no thorough observations of the current dune orientation and alignment with the existing climatic and environmental conditions. Thus, in this study, we examined the spatial patterns, geomorphology, orientation, and state of stability of the dunes in the KCCAD and analyzed their relationship to the contemporary precipitation and wind power. The wind regime data were collected from two sources—the Copernicus ERA5 reanalysis dataset (5,081 grid control points) and 36 National Oceanic and Atmospheric Administration (NOAA) weather stations—and used in sand rose calculations, according to Fryberger (1979). The regions that represented common dune

types were used in a series of 3D models to derive the link between the drift potential exponents and the orientation of the dunes. A significant goal of our study was to understand the environmental parameters associated with dune stability and environmental energy during the last 70 years.

2 Climate and geomorphic setting of the study area

The Köppen climate classification system assigns the label “Bwk” to the KCCAD region, referring to cold, dry, mid-latitude regions (Orlovsky, 1994; Maman et al., 2011). The aridification of this region of Central Asia occurred over a long period, from Tertiary to Pleistocene (Caves et al., 2016), coinciding with the uplift of the Asian high mountains (Abdrakhmatov et al., 1996), which cut off the rainfall supply from the south (Voigt et al., 2017; Hellwig et al., 2018; Fitzsimmons et al., 2020).

The current climate of this region is highly variable (Fitzsimmons et al., 2020), with long, hot, cloudless, and dry summers from May–September, with the average July temperature exceeding 30 °C. Winters in the south are pleasant and damp, whereas those in the north are cold and frosty. In January, the average temperature ranges from −10°C to 0°C

(Orlovsky, 1994; Lioubimtseva et al., 2005; Maman et al., 2011). Precipitation falls mostly throughout the winter and early spring, with more than half of it falling between December and April (Owen et al., 2018). In summer, both the deserts are dominated by the westerlies (Chen et al., 2008) and, to a lesser extent, the northerly winds associated with the southwestern edge of the Siberian anticyclone, while the Siberian High dominates the region in winter (Franz, 1972; Lydolph, 1977; Dodonov and Baiguzina, 1995; Orlovsky et al., 2005; Fitzsimmons et al., 2020) (Figure 2). Notably, the study area is located at the crossroads of the Asian monsoon belt (Dettman et al., 2001; Cheng et al., 2016), mid-latitude westerlies (Vandenberghe et al., 2006; Li et al., 2018), and high-altitude polar fronts (Machalett et al., 2008).

In general, the annual average wind speed in this area (KKCAD) is not higher than 5 m/s across, except for the Caspian coasts on the northern slopes of the Kopetdagh ridge (Orlovsky, 1994) and the Kulkuduk unit (Nappe formations near the Kulkuduk town) that have wind speeds of 6–9 m/s. By calculating the drift potential (DP) and resultant drift potential (RDP) values according to Fryberger (1979), for the short available time sequence of 2005–2008; Maman et al. (2011) concluded that the winds in the area portrayed the characteristics of a low-energy environment (less than 200 VU), with high wind variabilities and directionality index (UDI) values of ≤ 0.5 .

The annual precipitation in this area ranges from 110 mm in the Amu-Darya Delta to more than 300 mm in the Kopet Dag Range (Maman et al., 2011). Active aeolian formations stabilize if the wind speed is less than 6 m/s, annual average rainfall is more than 50–80 mm (Pye and Tsoar, 1990; Tsoar, 2005; 2008; Yizhaq et al., 2009), and there are no external stresses, such as animal burrowing or human trampling (Maman et al., 2021). Thus, the precipitation and wind statistics of this region indicate that the area can support appropriate plant cover. In this regard, most of the Karakum and Kyzylkum desert areas are dominated by vegetation and/or biological soil crusts (Maman et al., 2011), located in areas not affected by anthropogenic activity (Orlovsky, 2004).

In general, the contemporary and paleo-climate research on the interplay between fluvial and aeolian processes near the Syr-Darya and Amu-Darya rivers are quite restricted, in international as well as in literature available in Russian language. The raising of the Pamir-Alay Mountains created river channels that transect the Central Asian lowlands (Lioubimtseva, 2004). As a result, the paleo-Amu-Darya river and other paleo rivers (e.g., paleo-Syr-Darya, paleo-Murghab, paleo-Tedzhen, and other paleo-rivers coming from Tian Shan offshoots) deposited Neogene to Quaternary alluvium (Babaev, 1972; Nevodchikova, 1972; Walter and Box, 1983; Atamuradov, 1994; Thomas et al., 1999; Maman et al., 2011). Thus, present sandy dune forms in the KKKAD overlie Quaternary and Neocene alluvial deposits (Babaev, 1972; Nevodchikova, 1972; Maman et al., 2021).

In arid and semi-arid regions, linear dunes (vegetated and unvegetated) are the most prevalent desert dune forms, while barchans and transverse barchanoid ridges dominate the coastal dune fields (Inman et al., 1966; Wasson and Hyde, 1983; Pye, 1984; Illenberger, 1988; Pye and Tsoar, 2009; Craddock et al., 2015). Likewise, the Karakum and Kyzylkum deserts are dominated by vegetated linear dunes (VLDs), covering over 30% of the surface (Maman et al., 2021). Furthermore, VLDs are manifested in all different hierarchies (as simple, compound, and complex forms), covering the central part of both the deserts and manifested in

different complexities and orientations (Figure 2; insets 6 and 7); they are also found in coastal regions. In the past 2 decades, VLDs became a widely studied subject in the aeolian geomorphology due to their recognized significance as a marker of past climates when dunes were active (e.g., Roskin et al., 2011a; 2014; Robins et al., 2021) and a complex internal morphology that is being studied for the origin and evolution (Tsoar et al., 2004). Like that, VLDs play a key role in understanding paleo-environmental behavior of the region and its relation to contemporary system dynamics. Other dune types comprises smaller portions of KKKAD compared to VLDs.

Non-vegetated linear dunes are referred in this research as seif dunes. They are found in the coastal area of the Caspian Sea (Figure 2; insets 8 and 9), in simple and compound forms—when relatively small seifs superimpose the major seif body—and complex forms—when smaller seifs overlap the mega-barchanoid ridges. In this study, a smaller portion was observed in the active patches in the dipper desert, mostly coexisting with star dunes (Figure 2; insets 3 and 4). Barchans and barchanoid ridges in different hierarchies were observed in the coastal areas of the Caspian Sea and in different sections along the Amu-Darya River (Figure 2; insets 5, 10, 11, and 12). A large area of vegetated and partially active barchanoid ridges was recognized in the west-southwest part of the Karakum Desert (Figure 3; inset 11). Finally, parabolic dunes were recognized close to all water bodies in the area: the Caspian Sea coast, south of the Aral Sea, and in a wide region north of the Aydarkul Lake, existing usually as complex formations that superimpose the VLDs or develop within interdunal areas (Figure 2; inset 1 and 2). We assume that the variability and distribution of aeolian landscapes and deposits in the KKKAD reflect the wind regimes of the regional climate subsystems and general surface stability.

3 Materials and methods

The materials used in this study comprised of three main data types derived from weather stations, reanalysis algorithms, and satellite imagery. The data were extracted through multiple time-series and spatiotemporal statistical observations.

3.1 Data sources

3.1.1 Weather station wind data

The wind data were collected from sparsely spaced meteorological stations in Turkmenistan, Uzbekistan, and Kazakhstan, and acquired from the National Centers for Environmental Information¹ (hereinafter referred to as the NOAA weather stations). Only a few locations have been tracked for over a century, while other locations have considerable gaps and do not maintain continuous records, as commented by Cohen-Zada et al. (2017) (e.g., 40 years of data distributed across a 70-year span). Furthermore, numerous stations in the region effectively ceased operations because of major funding-cuts, following the collapse of

¹ URL: <https://www.ncei.noaa.gov/maps/hourly/>

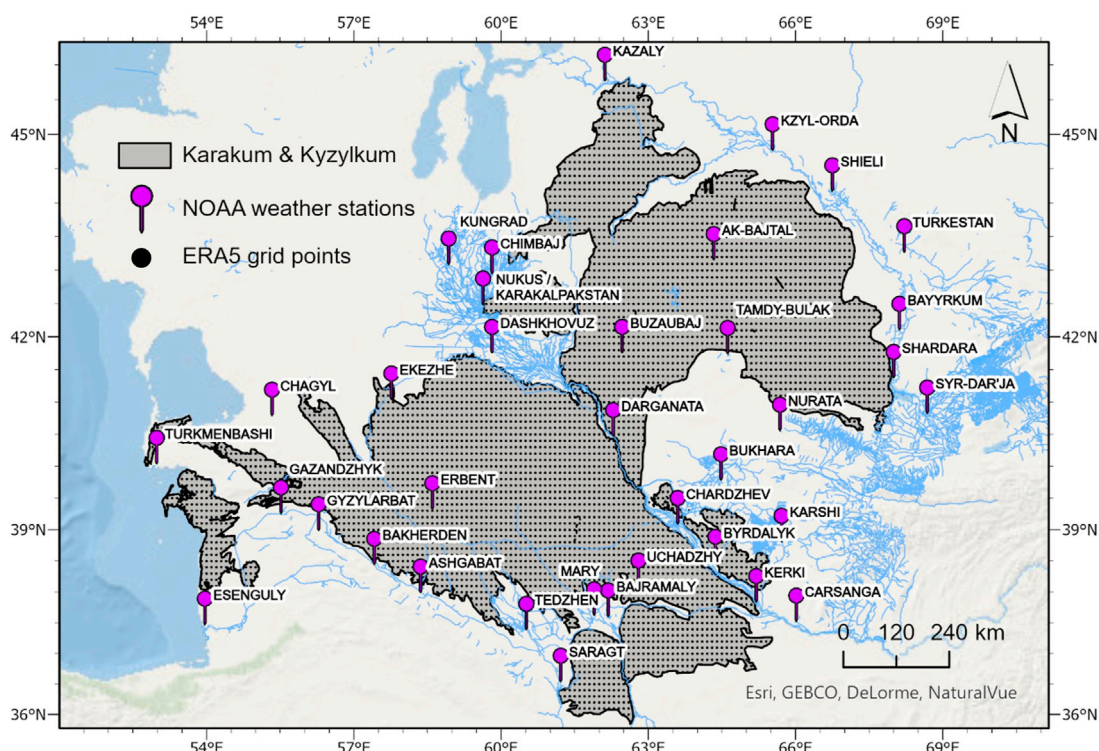


FIGURE 3 Spatial distribution of the 36 NOAA weather stations within and surrounding the research area and 5081 ERA5 grid control points. Data is available at National Oceanic and Atmospheric Administration (NOAA) web portal and the European Centre for Medium-Range Weather Forecasts (ECMWF) data server, respectively.

the Union of Soviet Socialist Republics (USSR) (Lioubimtseva et al., 2005).

For the study area, only eight stations had records of wind speed and direction at altitudes of 10 m above the ground for the period from 1 January 2010 to 31 December 2019. Hence, the region was observed in a wider context, and the data from 36 weather stations that were located both inside and at a close distance from the study region were considered (Figure 3). All the available wind readings for the statistical period were obtained, and the observations labeled as missing values, “-9,999” were omitted.

3.1.2 Wind reanalysis data

The reanalysis data were obtained using the European Center for Medium-Range Weather Forecasts (ECMWF)² ERA5 wind model. The ERA5 represents the latest Copernicus climate assimilation (4D-Var) and the model predictions in the ECMWF integrated forecast system (IFS) CY41R2. It contains the data of 137 hybrid sigma/pressure (model) levels, in the vertical and two spatial resolutions on single (0.25°), or land (0.1°) levels, with a consistent view of the evolution of land variables since 1 January 1950, updated regularly until today. The adopted spatial and

temporal resolutions of the attained datasets were 0.1° × 0.1° and 1 h, respectively. In this study, we exploit this dataset to accomplish several objectives: analyzing a 10-year dataset from 1 January 2010, to 31 December 2019, to link the dune orientation with the resultant drift direction (RDD) in the region, and a 70-year data set spanning 1 January 1950, to 31 December 2019, to understand the energy of the depositional environment and its spatiotemporal distribution in the study area.

The azimuthal (U) and meridional (V) components of the entire time-series of the 10-m height wind were processed to calculate the speed and direction of the wind, using the following equations:

$$\begin{aligned}
 \text{Speed} \left(\frac{m}{s} \right) &= \sqrt{U^2 + V^2} \\
 \text{Direction} \left(^\circ \right) &= \arctan \left(\frac{U}{V} \right)
 \end{aligned}
 \tag{1}$$

Wind speeds are subsequently transformed in units of knots and monitored for 16 compass directions according to the processing criteria of the Fryberger (1979) sand rose calculations.

3.1.3 Precipitation data

The precipitation data were obtained using the Climate Change Knowledge Portal (CCKP) of the World Bank Group (WBG)³. The

² URL: <https://www.ecmwf.int/en/forecasts/datasets/reanalysis-datasets/era5>

³ URL: <https://climateknowledgeportal.worldbank.org/>

TABLE 1 Spatial resolution attributes for the remote sensing data used in this study.

Product	Pixel size
Sentinel-2	10 m
Bing Aerial Imagery	up to 30 cm
Esri Basemap	up to 7.5 cm
Esri Terrain layer	up to 1 m
ALOS PALSAR	12.5 m
SRTM 1	30 m

data were obtained from the Climatic Research Unit gridded Time Series (CRU TS), produced by the CRU of the University of East Anglia (UEA), and is accepted as the most widely used observational climate dataset (Harris et al., 2020; CCKP, 2021). In this dataset, the data are displayed on a 0.5° latitude × 0.5° longitude grid for all the land areas, except Antarctica. The CRU TS version 4.05 gridded dataset was produced from observational data and contained quality-controlled temperature and rainfall readings from hundreds of weather stations worldwide and different derivative products, such as monthly and long-term historical climatologies (Harris et al., 2020). The average annual rainfall for the previous four climatic cycles (1901–1930, 1931–1960, 1961–1990, and 1991–2020) was acquired from the CCKP gateway page, to study alterations in spatiotemporal distribution of precipitation over the KKCAD and its relation to dunes stabilization agents.

3.1.4 Satellite imagery data

We incorporated numerous forms of satellite data, including optical imagery and several digital elevation models (DEMs) (Table 1). Satellite data were utilized to determine the dunes activity/stability, orientation, and dunes peak height, in order to develop and comprehend the relationship between the behavior of different dune types across the desert for different wind attributes.

3.2 Methodology

Previous studies demonstrated that sand seas and aeolian formations can provide records of current and previous climatic shifts and conditions (Lancaster, 1995; Muhs and Holliday, 1995; Roskin et al., 2011b; Leighton et al., 2013) and may be a regional indication of prior and current wind directions and strength (Lancaster, 1995; Muhs and Holliday, 1995; Leighton et al., 2013; Lindhorst and Reimann, 2021; Robins et al., 2021). The regional sand flow results could be approximated using three methodologies (Pye and Tsoar, 2009): by considering the a) wind velocity data, with a sand transport rate equation, such as that proposed by Bagnold (1941); Fryberger (1979); b) sandstorm duration and direction records (Dubief, 1952); and c) size and orientation of aeolian bedforms and sand streaks (Cohen-Zada et al., 2017). The drift potential is assumed to be an essential factor determining the formation and growth of dunes provided sufficient wind records are available (Zamani et al., 2020; Hu et al., 2021), and the first approach (use of wind chronicles) can yield the results for any

period and particle size (Pye and Tsoar, 2009). As this is not always the case in remote desert areas, we tested the data sources to identify which method (reanalysis or weather measurements) was more accurate. The DP and sand rose exponents, RDP, RDD, and wind directionality index (UDI = RDP/DP) were calculated using the established MATLAB algorithm, according to Fryberger (1979) and Zamani et al. (2020). The data from 36 NOAA weather stations for 1 January 2010, to 31 December 2019, were compared to the nearest grid point of the ERA5 reanalysis assimilated dataset. Based on obtained findings, the relationship between dune orientation and DP was further examined, in reference to the ERA5 wind data. Figure 4 summarizes the overall workflow of this study.

3.2.1 Multidimensional raster analysis

In this study, we used DP and UDI to analyze the alterations in the wind energy environments and dune activity during 1950–2019. In general, the data gathered for the same rasterized area along the temporal dimension are referred to as multidimensional data. This implies that, for each grid point or series of points, the value of the observed variable is given at a certain moment in time, and like that observed for the desired time extent. Essentially, the data was layered and stacked according to their spatiotemporal characteristics and statistically evaluated for the total of 355,670 monitored segments. Using the advantages of multidimensional data and spatiotemporal assessment, the original values for each grid point were saved, rather than interpolated, as carried out in many previous examinations and interpretations of DPs (e.g., Maman et al., 2011; Hu et al., 2021). Separate space-time cubes were built for DP and UDI (excluding circular variables and their resultant powers); notably, the data of these parameters were mined for the average values and linear trends over time. Additionally, the data were taken through Hot Spot Analysis (hereinafter referred to as HSA), to calculate the Getis-Ord G_i^* statistics, and time-series partitioning around medoids (PAM) clustering (hereinafter referred to as TSC).

The HSA combines two statistical approaches: the Getis-Ord G_i^* (Getis and Ord, 1992; Getis and Ord, 1996; Ord and Getis, 1995; Mitchell, 2005; Peeters et al., 2015) and the Mann-Kendall trend test (Mann, 1945; Kendall, 1975), to investigate how geographical groupings of extreme values evolve (extreme high values = hot spots; extreme low values = cold spots). The Getis-Ord G_i^* statistic is an adaptation of the General G-statistic (Getis and Ord, 1992), a commonly used method for quantifying the degree of spatial autocorrelation over an area (Peeters et al., 2015). After the space-time HSA was completed, each bin in the input raster was assigned a z-score, p-value, and hot spot bin categorization. The Mann-Kendall trend test was then used to examine the hot and cold spot patterns. Note that for a feature to be a statistically significant hotspot, it must have a high value and be surrounded by additional features having high values.

The TSC algorithm (Montero and Vilar, 2014) can be used to determine the related locations in a space-time cube accurately; additionally, the algorithm divides them into distinct clusters, consisting of members who have similar time-series characteristics. In this context, the time series are comparable, if their values tend to grow and fall at approximately the same time and are proportionate. This clustering begins with the development of a matrix, which is then clustered using the k-medoids technique (Kaufman and Rousseau, 2009), commonly known as the PAM

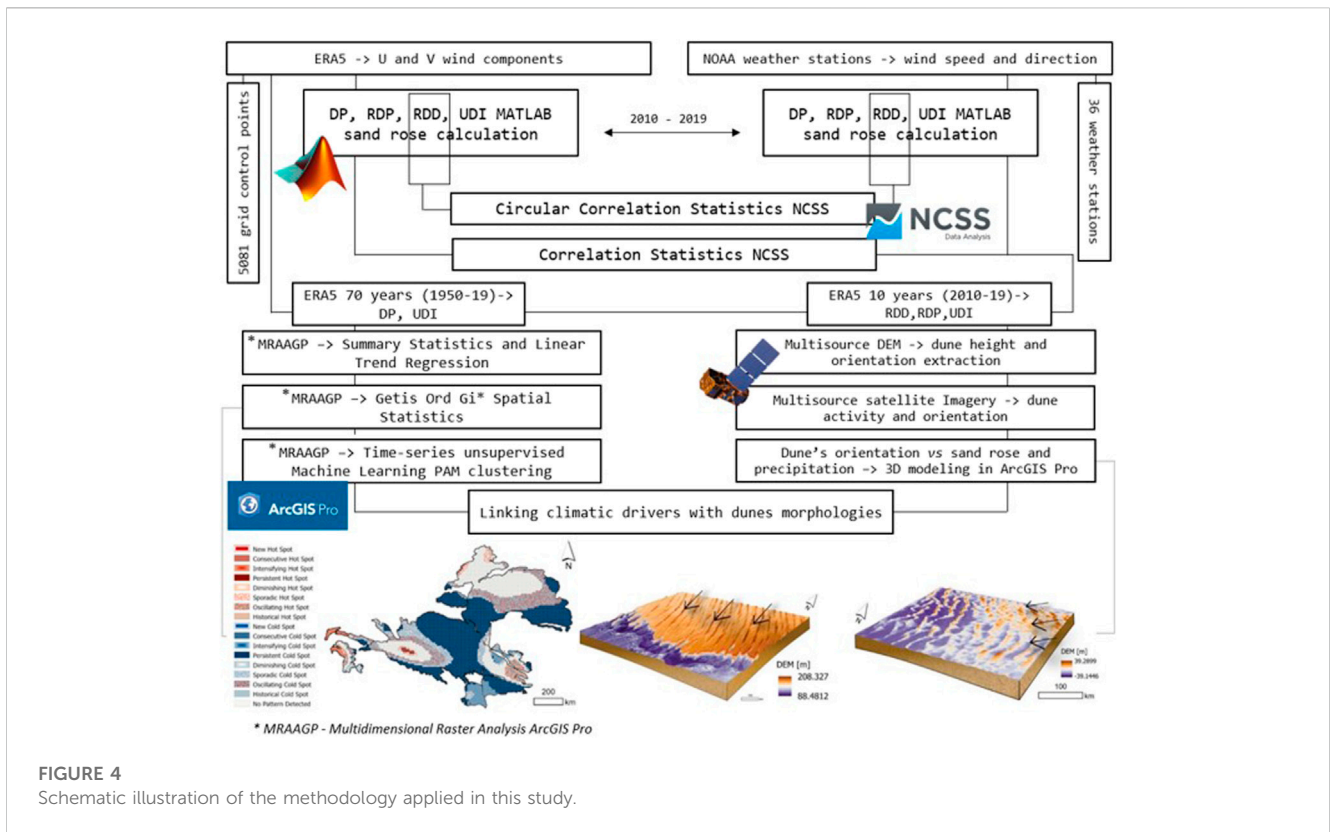


FIGURE 4
Schematic illustration of the methodology applied in this study.

algorithm. This model locates the clusters inside a matrix, whose members are similar to those of other clusters, by selecting random locations to represent each cluster. More information on the multidimensional raster analysis, mentioned performances, and explanation pertaining to the classes assigned for HAS can be obtained from the Esri’s official website⁴.

3.2.2 Dune orientation versus drift potential (DP) exponents

The orientation of the dunes in KKCAD region and their current morphological profiles were extracted from multiple DEM sources and linked to the DP, RDD, RDP, and UDI values calculated for the statistical period of 2010–2019. The procedure was repeated for the VLDs, seif, barchan, barchanoid, star, and parabolic dunes surveyed in different portions of the KKCAD. As the coastal region had a complex dune setting, some incompatibilities existed between the dune orientation and RDDs, referring to a better correlation between the superimposed formations and the obtained RDDs, or the underlying mega-dunes. Thus, the wind data acquired for the active Caspian coastal region were split into the Northern Hemisphere seasons, namely, winter (November–February) and summer (May–August), as well as the geomagnetic time hours of sampling of the reanalysis data (06:00 h and 18:00 h) (Cohen-Zada et al., 2017), for the same statistical period. As the segment of different dune types varied significantly, we used Google Earth Pro, whose DEM model is based on the Shuttle Radar Topography

Mission (SRTM) data (30 MP resolution), along with other sources (Table 1). For each dune type, six different dune locations were chosen, to derive relationship with contemporary winds. The average dune height for each field was extracted based on ten different, random, and approximately 10-km long intersects that were perpendicular to the crest lines of the dunes. The average RDPs were extracted for the same areas of interest (AOIs). Both the bed height and RDP values for the examined dune types were plotted and related to the UDI. Figure 4 portrays an example of a 3D assessment for determining the bed heights and orientation versus overlaying the resulting drift vectors and their powers.

4 Results

Our statistical observations of the wind data acquired from the 36 NOAA weather stations within and around the study area for the 2010–2019 period (Figure 5), reveal that the winds with velocities less than 6 m/s (included) and those flowing from the North and East dominated the area. The DPs calculated for the weather stations and the ERA5 reanalysis control points were statistically verified using the NCSS software⁵.

According to Fryberger (1979), winds with minimum velocity of 12 knots or ~6.2 m/s are sufficient to generate sand saltation and form dunes in sand-reach environments. As such, they are referred to as erosive henceforth. For each of the 36 NOAA weather stations,

4 URL: <https://pro.arcgis.com>

5 URL: <https://www.ncss.com/>

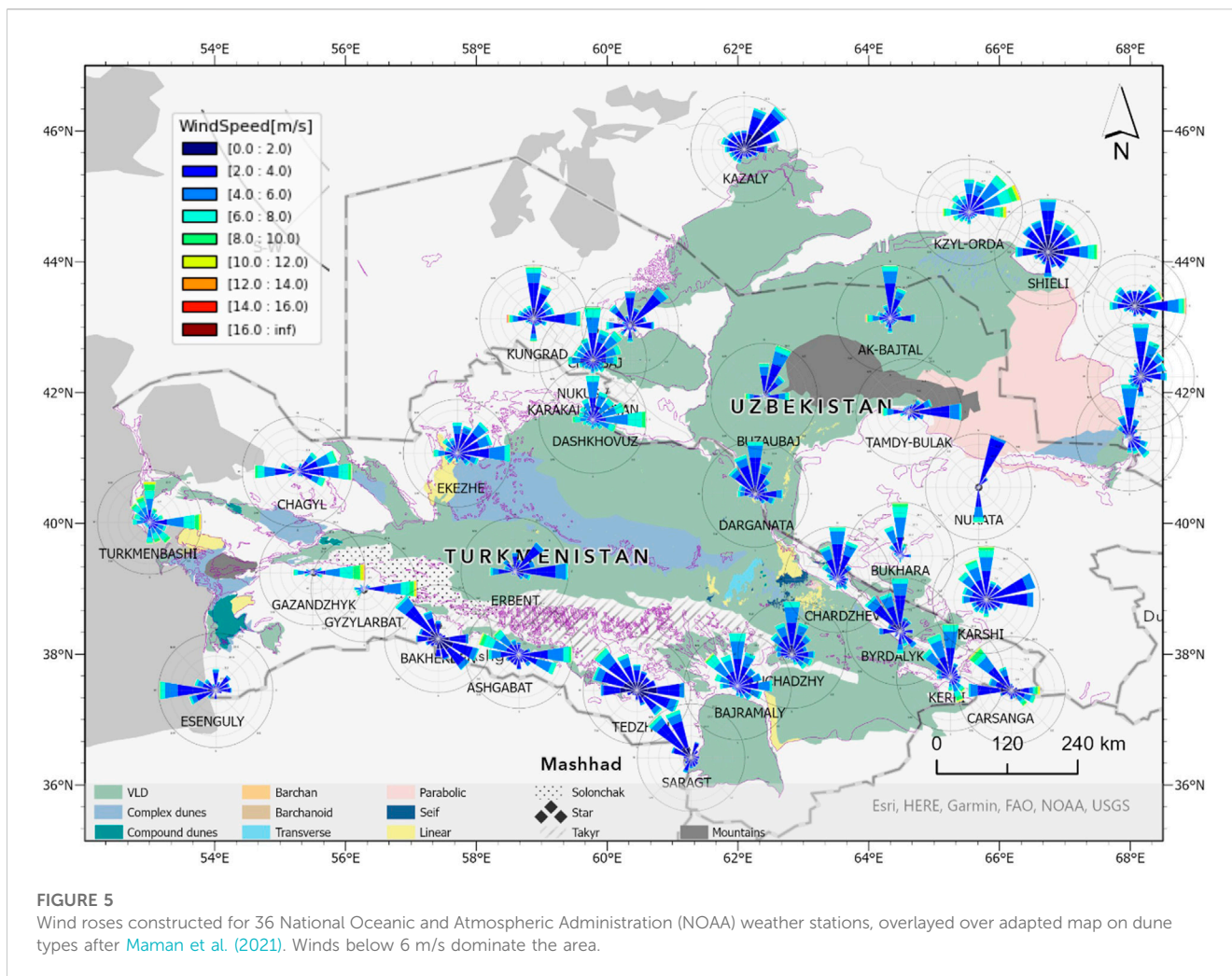


Figure 6 portrays the percentage of no wind or low wind periods (referred to as “calms” in this study), along with the percentage of those surpassing the minimal sand saltation threshold, exclusive of winds between two mentioned categories. Based on the stationary-based meteorological reading, all investigated sites portrayed a significantly higher percentage of calm intervals than those that had an adequate force to commence erosion. The percentage of calms ranged from 1.4% (Dashoguz weather station) to 69.4% (Nurata weather station), which, in a 10-year-period, accounts for up to ~7 years of low wind activity. Only 8 of the 36 sites had erosive winds blowing more than 10% of the overall monitored duration.

Figure 7 depicts the descriptive statistics and correlation coefficients for two datasets on DP variables calculated from the data acquired from the 36 weather stations and the closest ERA5 grid control points. The RDDs and their RDPs exhibited the greatest correlation coefficients between the examined DP components (0.59 and 0.57, respectively), which indicated a low to moderate correlation. In addition, it was easy to deduce from the correlation coefficients and *p*-values that there was a low correlation between the observed variables. However, the DP values from both the weather stations and the reanalysis data classified the majority of the KKCAD region as a low-energy environment, with DP values of

less than 200 VU. Based on the studied aeolian profiles and active dune orientation, it can be assumed that the local sand transport patterns in the KKCAD deviate considerably from those predicted using weather-station data. Such performance is generally attributed to one of the three dominantly recognized factors: low spatial and/or temporal resolution of measurements, topographical dependencies, or secondary atmospheric circulations (Pye and Tsoar, 2009; Cohen-Zada et al., 2017). Therefore, the ERA5 reanalysis-assimilated dataset was identified as a more relevant wind data source for correlating dune morphologies and climatic drivers in the KKCAD.

4.1 Spatiotemporal patterns of drift potential (DP)

The spatial patterns of the DP and UDI in the KKCAD are shown in Figure 8. According to Fryberger and Dean (1979) and the worldwide studies that include KKCAD region, the UDI values of 0–0.3, 0.3–0.8, and 0.8–1 represent high, intermediate, and low wind variabilities, respectively, whereas the DP values of 0–200, 200–400, and 400–600 VU represent low-, middle-, and high-energy environments, respectively.

Descriptive Statistics & Correlation

Variable	N	Mean	Standard Deviation	Minimum	Maximum	Pearson Correlation	P-value
DP_NOAA	36	135.24	138.51	1.69	631.22	0.2813	0.0966
DP_ERA	36	59.31	61.72	0.23	204.21		
RDP_NOAA	36	54.40	74.73	0.51	403.41	0.5666	0.0003
RDP_ERA	36	23.24	28.38	0.13	108.60		
UDI_NOAA	36	0.47	0.23	0.12	0.99	0.1666	0.3316
UDI_ERA	36	0.44	0.22	0.06	0.99		

Circular Data Correlation

Variable	N	Mean Direction	Circular Variance	Circular Standard Deviation	Von Mises concentration (Kappa)	Correlation coefficient	P-value
RDD_NOAA	36	335.64	0.5373	71.13	1.05	0.5864	0.0022
RDD_ERA	36	163.52	0.6716	85.50	0.69		

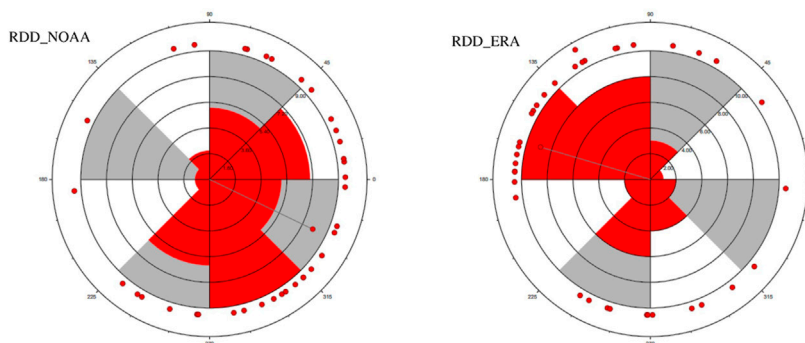


FIGURE 6

Sand Roses for 36 National Oceanic and Atmospheric Administration (NOAA) weather stations in relation to ERA5 grid points. Sand Rose follow the location of wind roses depicted in Figure 5. The green, red, and blue color of the information window below each rose stands for Turkmenistan, Uzbekistan, and the stations located in Kazakhstan, respectively. The circular correlation between two variable resultant drift vectors is 0.5864, revealing a low to moderate correlation.

Corresponding to the average UDI raster over the 70-year period considered in this study and 5,081 grid control pixels per year, no apparent rising or declining gradient for the directionality variable was observed. The UDI trend statistics demonstrated that erosive winds did not deviate significantly from their primary directions over the same data period, revealing the constancy of multidirectional winds in the region. The above-average values of DP were observed in the takyr-solonchak margin with the Karakum Desert’s southwest, which extended to the Caspian coastal dune fields—where the value can reach over 600 VU with the intrusion of stronger winds, and in the southeastern region. These regions were also areas represented by positive linear trends for calculated DPs, and were probably the most dynamic sections of the KKCAD.

In the Kyzylkum Desert, the DP values above 200 VU were observed only in a small portion of the northern desert margin. Most of the area either did not have a prevalence, or revealed a negative trend over the 70-year span in the annual drift potential calculation. Notably, most of the region sits in a low-energy environment setting, with high to moderate wind variability, represented by a DP of less than 150 VU, and a UDI dominantly below ~0.4. Unidirectional winds with low wind variability were only observed in the Caspian Sea coast (in the western part of the Karakum Desert) and around the Aydarkul Lake (on the eastern margin of the Kyzylkum Desert).

In addition to the discussed activity in the coastal zone, the active formations were only observed as small, sparse, and very irregularly-shaped patches located in random areas that were not influenced by the local topography. Among them, the larger active field in the Kyzylkum Desert is seen as a complex intermittent dune field in the SE margin, stretching as a discontinuous meridional chain of active but small aeolian profiles, and ending before the Amu-Darya River. These fields have average DP values ranging between 50- and 200- VU and high wind variabilities (UDI<0.3). As observed in our study, the trend of DP changes in these regions was predominantly negative, indicating a decrease in the annual values over the observed period. Active patches in Karakum are represented by seif, star, and transverse dunes extending from the E-NE takyr border, pointing NE to the Amu-Darya River (Figure 2, intersecting zone between window 6 and window 4,5). The winds were highly variable (mostly 0.1–0.4), with the DP values exceeding 200 VU only in the minor eastern part of the dune field. The trend of the DPs was similar to that observed in Kyzylkum, where negative changes dominated.

The DP values were further statistically assessed using the HSA and TSC methods. As suggested in chapter 3 (visual representation given in the methodology workflow), the HSA method was used to indicate the areas where features with high or low values clustered geographically, by examining the behavior of the surrounding

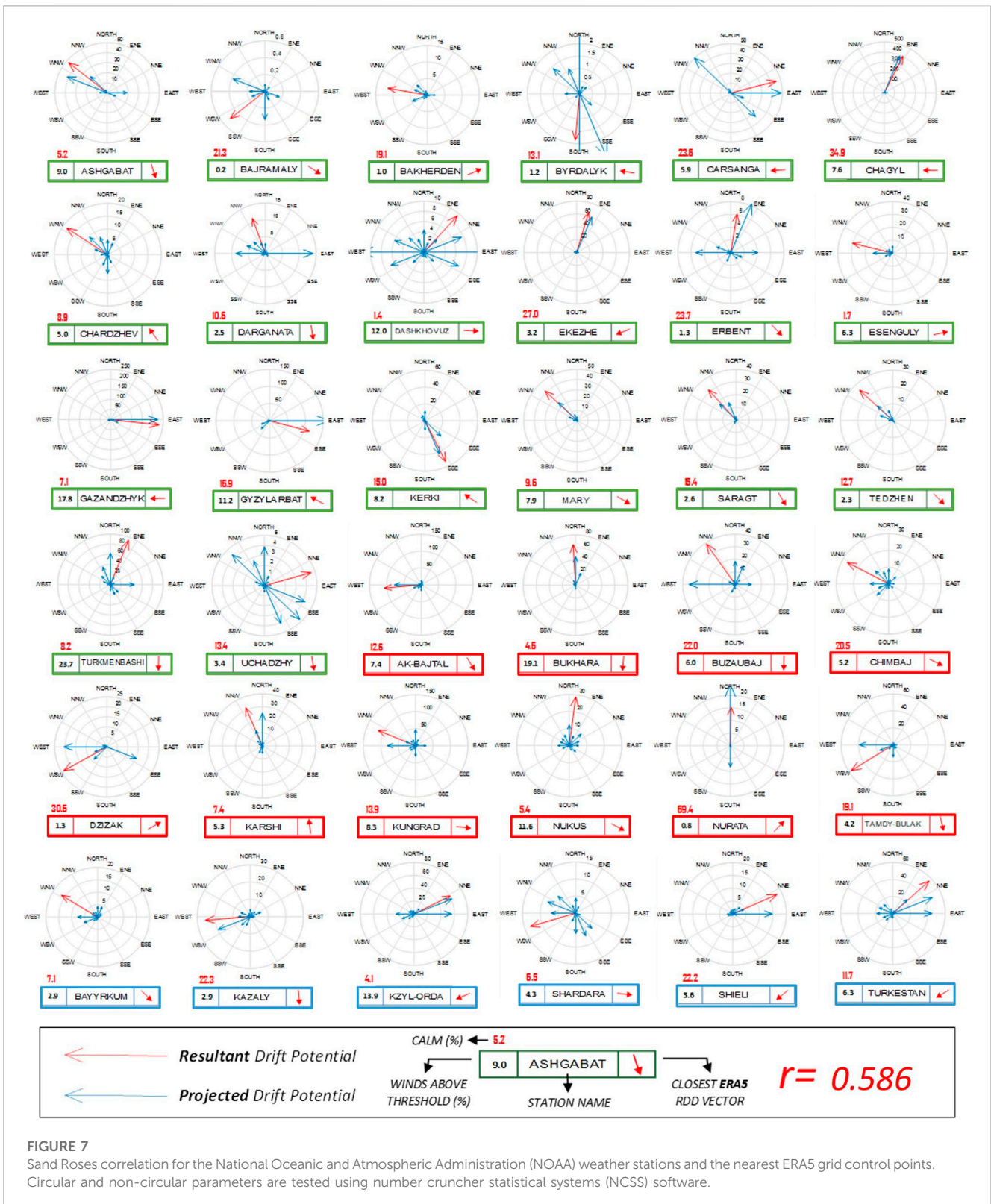


FIGURE 7 Sand Roses correlation for the National Oceanic and Atmospheric Administration (NOAA) weather stations and the nearest ERA5 grid control points. Circular and non-circular parameters are tested using number cruncher statistical systems (NCSS) software.

features; the study area was categorized using the trend z-score and *p*-value for each location. The local sum for a feature and its neighbors was compared proportionately to the total of all features. If the calculated local sum differed significantly from the predicted local sum, and the difference was extremely large to be

considered random, a statistically significant z-score was calculated. The pattern in the KKCAD revealed that cold spots dominated the region, referring to the pixels having principally low DP values that were statistically significant cold spots for 90% of the time-step intervals (with no discernible trend). The statistical assessments of

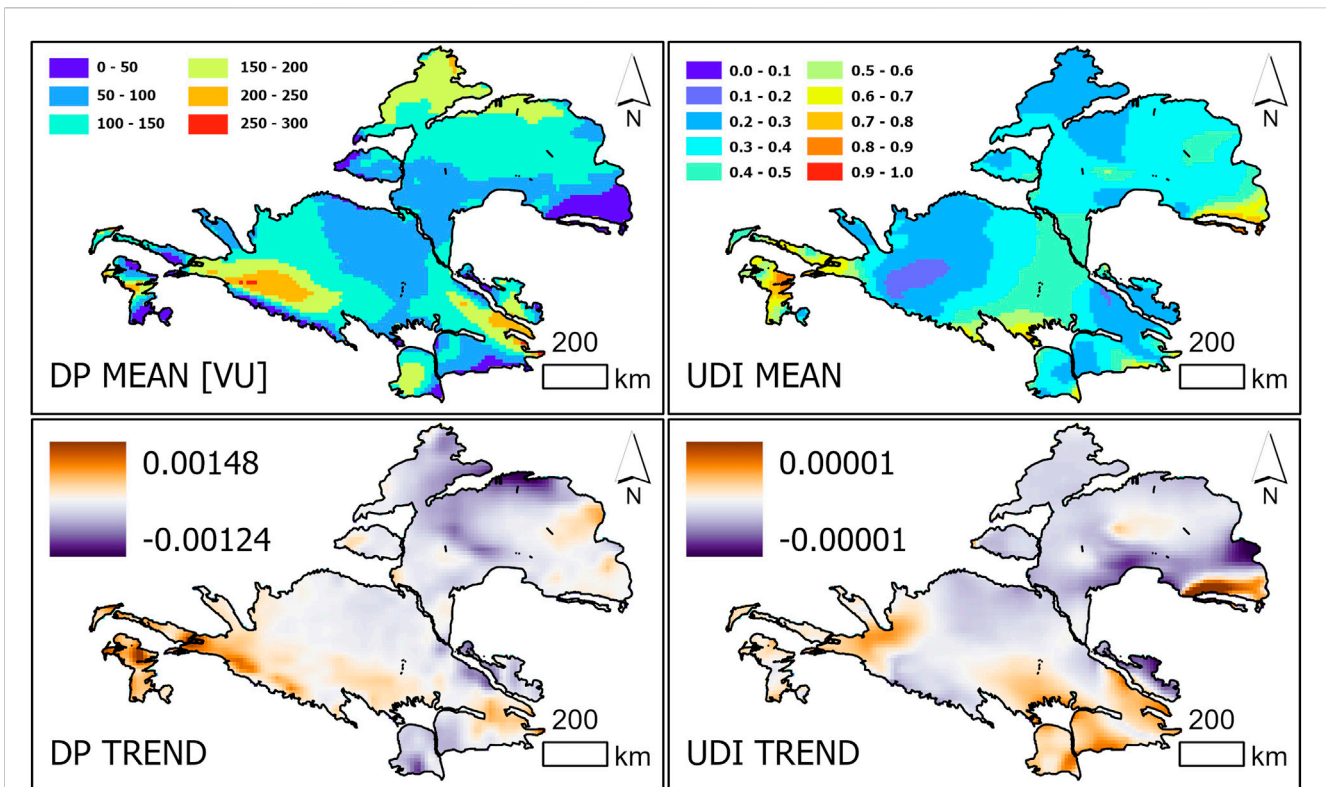


FIGURE 8 Space-time cube statistical assessment. Average drift potential (DP) and wind directionality index (UDI) values, and their linear trends of change over 70 years.

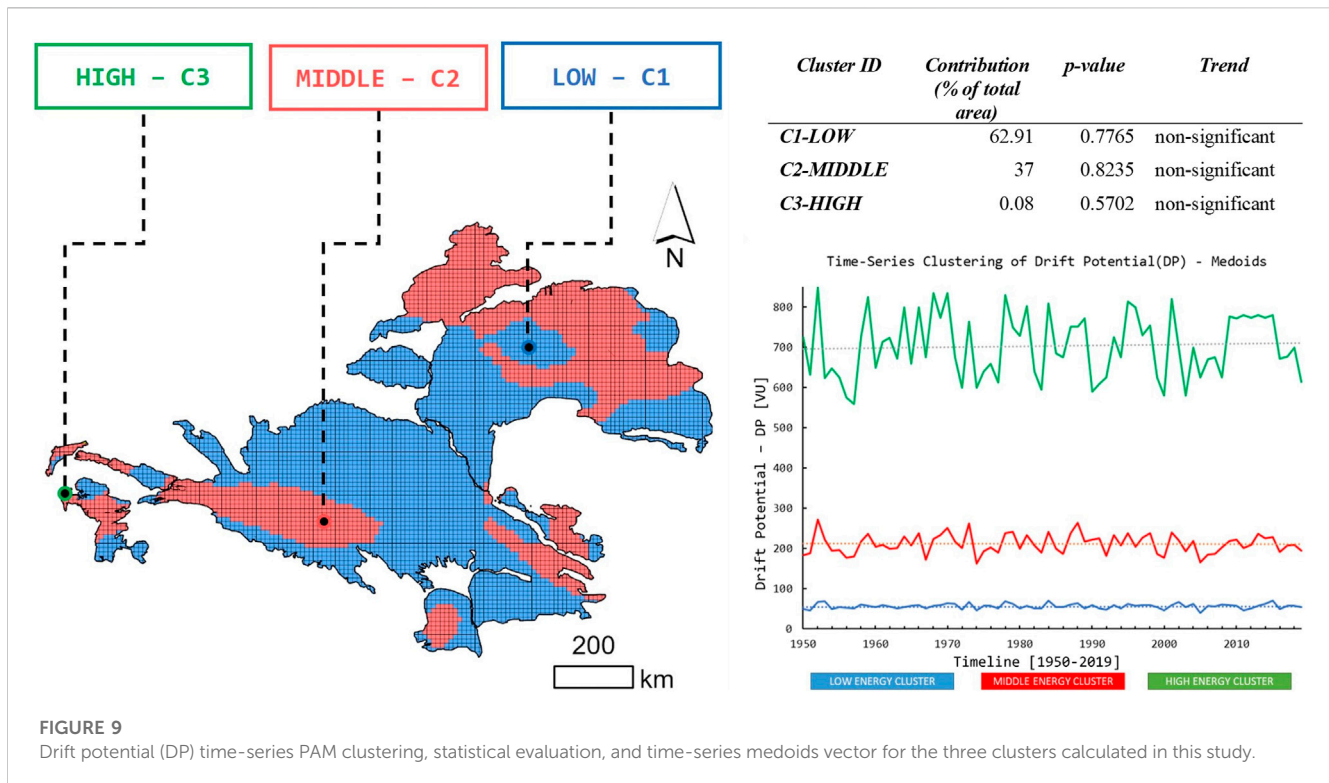
TABLE 2 Emerging hot-spot analysis: pixels summary.

Pattern type	Number of pixels	Contribution (%)
Oscillating Hot Spot	158	2.71
Sporadic Hot Spot	100	1.71
Persistent Hot Spot	36	0.62
Intensifying Hot Spot	98	1.68
New Hot Spot	2	0.03
No Pattern Detected	1309	22.41
Intensifying Cold Spot	247	4.23
Persistent Cold Spot	2486	42.57
Diminishing Cold Spot	45	0.77
Sporadic Cold Spot	447	7.65
Oscillating Cold Spot	864	14.79
Historical Cold Spot	48	0.82

the pixels after the HSA are presented in Table 2. The coastline region was previously identified as a zone with a positive trend, by conventional linear regression, and the HSA statistics assigned it a similar category of intensifying hotspots. An intensifying hot spot was a statistically significant hot spot for 90% of the time-step

interval, including the final time step. Furthermore, the total intensity of the clustering of high values in each time step increased, and this increase was statistically significant. In addition, sporadic and oscillating cold spots were observed in the region that represented the locations that were statistically significant cold spots for less than 90% of the time-step intervals. The distinguishing factor among these two is that the sporadic spot has never been a statistically significant hot spot with high values in prior time-step intervals, while the oscillating one had a history of being a statistically significant hotspot during previous time steps. In KKCAD, sporadic cold spots generally surrounded the oscillating cold spots.

The TSC results represented the locations in which the DP values and their temporal vectors were correlated across a spatio-temporal dimension for 70 years period. As shown in Figure 9, three clusters simulate an optimal number of classes, similar to Fryberger's (1979) (low-, middle-, and high-energy environments). The TSC method enabled us to group most of the pixels where the DP values were no more than 100 VU. Note that the final clustering was performed based on both the original and neighboring values and their spatiotemporal variations and correlations. Only extreme pixels were extracted into the high-energy cluster (barely visible in Figure 9, owing to the scaling factors and areal extend of only 0.08% of the total area), and the zone with middle-energy was extended. Notably, the large northern part of the Kyzylkum Desert was assigned the same class as the previously discussed dynamical coastal region with other pixels that had higher DP values, most



probably explained by similar changing aspects over the 70-year period. A large portion of the middle-energy cluster in the eastern Kyzylkum area overlays an extremely complex geomorphic setting, where small, dense, and vegetated parabolic-like dunes superimpose the VLDs and their interdunal areas.

The zones within the KKCAD previously considered to have positive trends are likely to portray a slight increase in the DP and eventually, gradient deeper into a middle-energy environment. The wind over active patches portrayed a slight drop in the DP values, referring to a possible decrease in its velocity, resulting in the strengthening of dune stabilization in this region, if no additional disturbances will occur in the region (e.g., anthropogenic pressures, intensive storm events). To derive a more precise conclusion, one should look closely at much smaller AOIs within a large area of the KKCAD and derive a link to the underlying aeolian performances, using better spatial resolution and field confirmations. In conclusion, most of the area maintained its recognizable dynamics, while remaining within a low-energy environmental setting; notably, we observed no distinct areas that portrayed drastic DP decreases or increases during the study period.

4.2 Associating dune orientation and resultant drift direction (RDD)

4.2.1 Certain dune types

In this study, the morphologies of the dune in the KKCAD region were analyzed using several remote sensing (RS) and geographic information system (GIS) data sources, to assess the dune types in the region and the existence of superimposed features, determine their directions, and estimate their dunes pick heights.

Due to the vastness of the study region, it is difficult to characterize the morphologies of all the dunes identified at the local scale in a single comprehensive study; hence, the research is focused on dunes that are emblematic of the region. The calculated RDDs and their RDPs (Figure 10) allowed us to evaluate whether the contemporary winds in the study area had the necessary force and trajectory to saltate sand grains and generate dunes.

Figure 11 depicts a section of the studied dunes and the accompanying DP estimates, while Figure 12 depicts a schematic summary of the wind performances over examined dune types. The predominant aeolian forms are VLD, seif, barchan, barchanoid ridge, parabolic, and star dunes. In various hierarchies (simple, compound, and complex), these forms appeared in the interior and coastal regions. The three primary entrance routes for winds powerful enough to reconfigure sandy deserts, were from the North-West, North, and Northeast directions. Even though westerlies were common, they appear with lower velocities compared to north-easterly winds. Smaller intrusions were noticeable at the eastern edge of Karakum, where the wind flow was from the Pamir Mountains, deflected by the northwesterlies to the southeast.

The VLDs (the most common dune type) in the Karakum and Kyzylkum deserts appeared at heights of 15–50 m, with resultant drift potentials of 10–50 VU, for high–moderate wind variability ($0.15 < \text{RDP/DP} < 0.45$). They were formed across the Caspian coastal region as simple formations. Moving east, they merged with parabolic dunes, after which they occupied the interior of the KKCAD region, comprising the entire region of the Kyzylkum Desert and the bulk of the Karakum. The internal section was represented by complex and compound formations, wherein mega VLDs were superimposed by parabolic dunes, as seen in the eastern

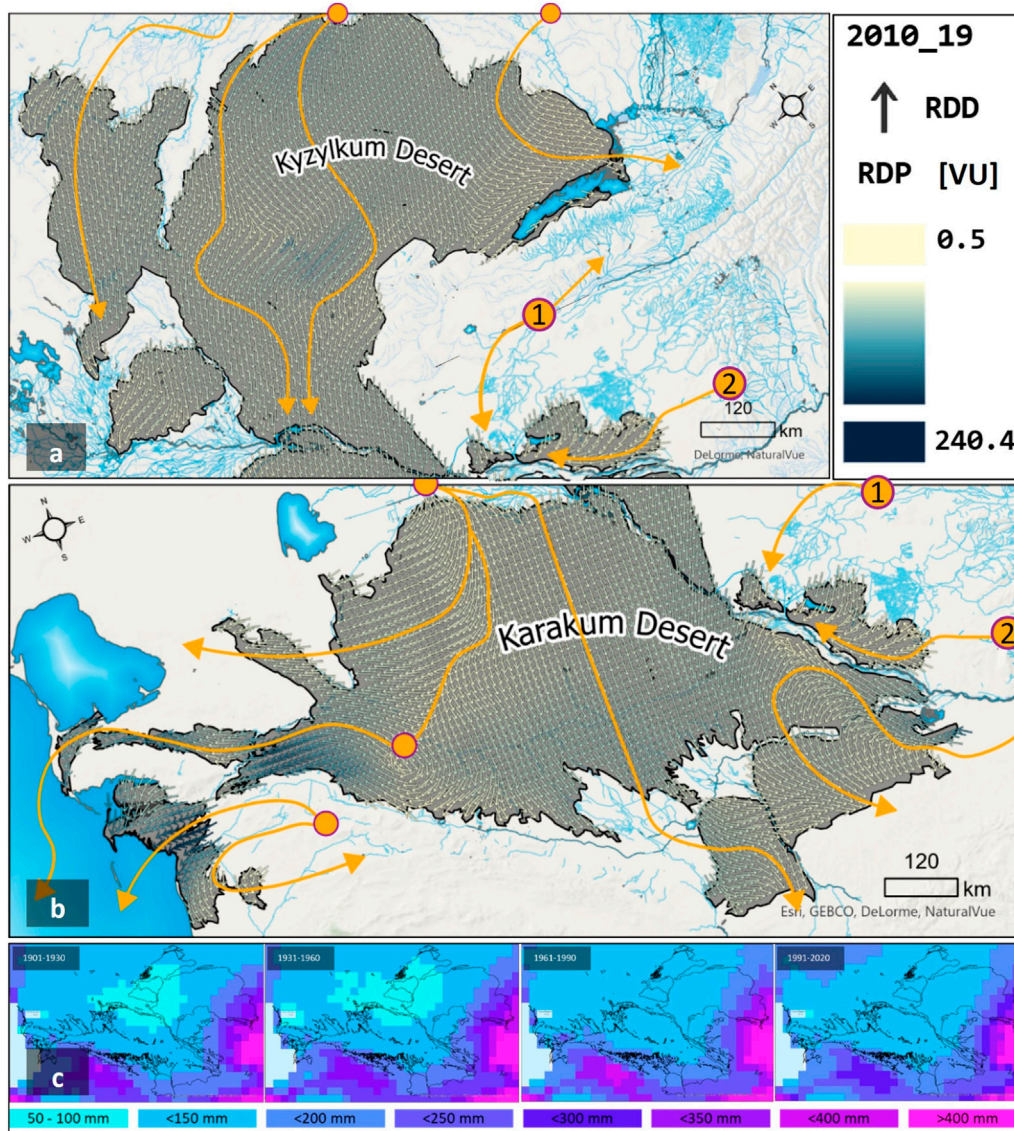


FIGURE 10

Sand roses resultant drift direction (RDD) for 5081 ERA5 grid control point over the Kyzylkum (inset a) and Karakum (inset b) Central Asian deserts (KKCAD), calculated for the statistical period 2010–2019. The color of the RDD vector represents the intensity of their powers, with a maximum reaching only 240.4 VU. The yellow arrows represent the manually inserted discernible wind drift trajectories, whereas the rings represent the significant intersections across the region, where erosive winds deviate from their primary routes. A four-climatic-precipitation-cycles composite (inset c), spanning from 1901 to 2020, emphasizes a sufficient amount of rainfall over the whole study area.

part of the Kyzylkum Desert (Figure 3; window 2), and by other linear dunes with different orientation, as seen in the central Karakum (Figure 3; window 6). Satellite images illustrated the NNW-SSE trends of the mega VLDs, with NNE-SSW trends of linear (as seen in Karakum) and S-N trends of parabolic (as seen in Kyzylkum) dune superimpositions. Where the middle Kyzylkum is divided by a hilly ridge known as the Kulkuduk unit that lies perpendicular to the incoming wind direction (Figure 2, intersecting zone between windows 7 and 4,5), the effect of topography on near-surface airflow is evident. Thus, several variations from the largely characterized directions of the discussed VLDs were seen in dune field surrounding the unit.

The orientation of the VLDs in the Caspian coastal region (Figure 11) matches with the summer drift directions (May–August). As this segment of the KKCAD is partially stabilized by biogenic crusts, the crust flourishing in more humid intervals during the year may preclude the entire annual remodeling of the accessible desert. As a result, the dry season could have fewer biogenic crusts, allowing more sand to be accessible for erosion and reshaping, which may explain the stronger alignment between dune orientation and drift directions computed for the total of the summer winds. This is a clear indication of fluctuations in wind speed and direction, precipitation, and/or seasonal variations in sand availability in the region (Courrech du Pont et al., 2014; Gao et al., 2015). Nonetheless, the results indicated the low-energy

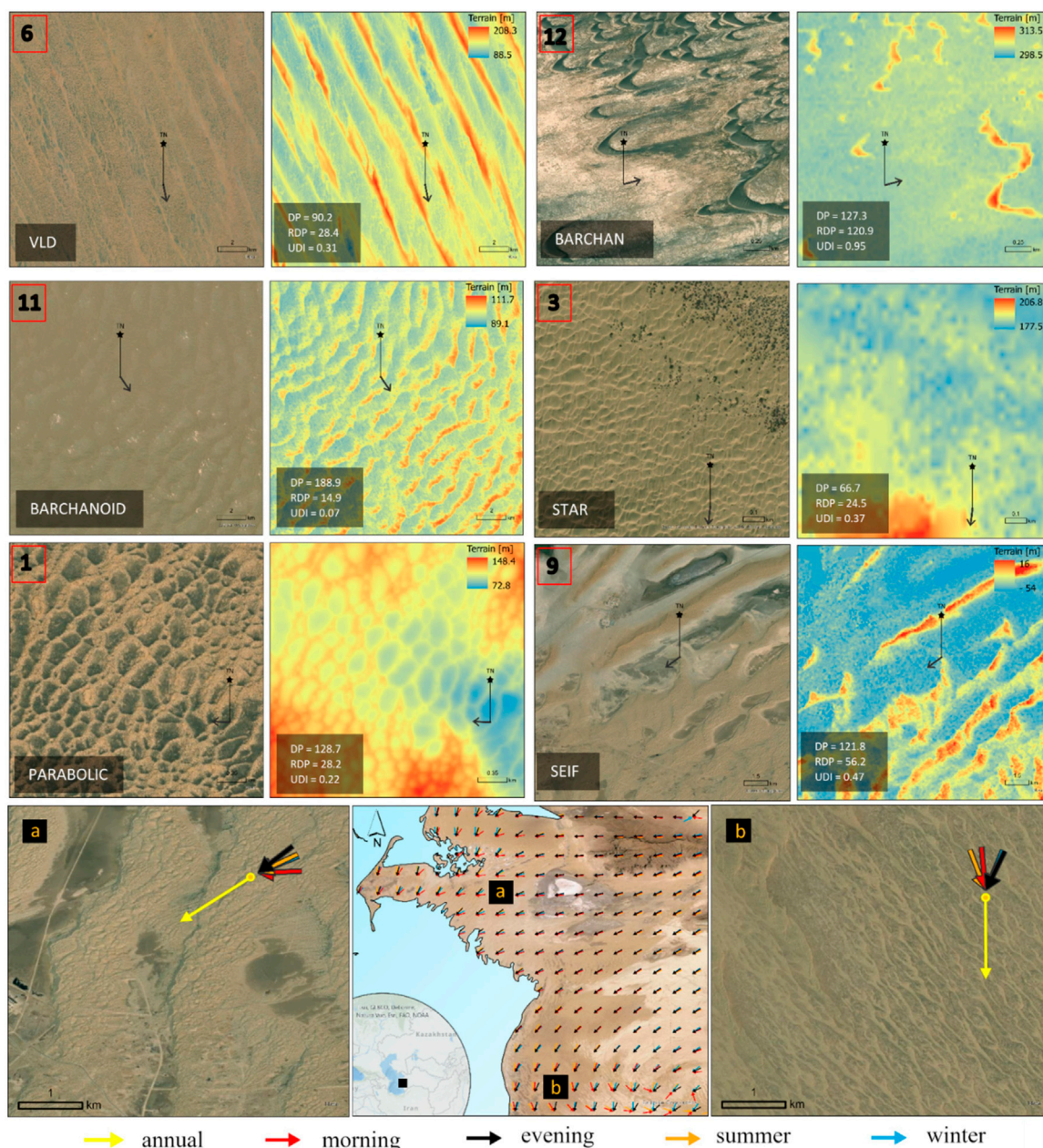
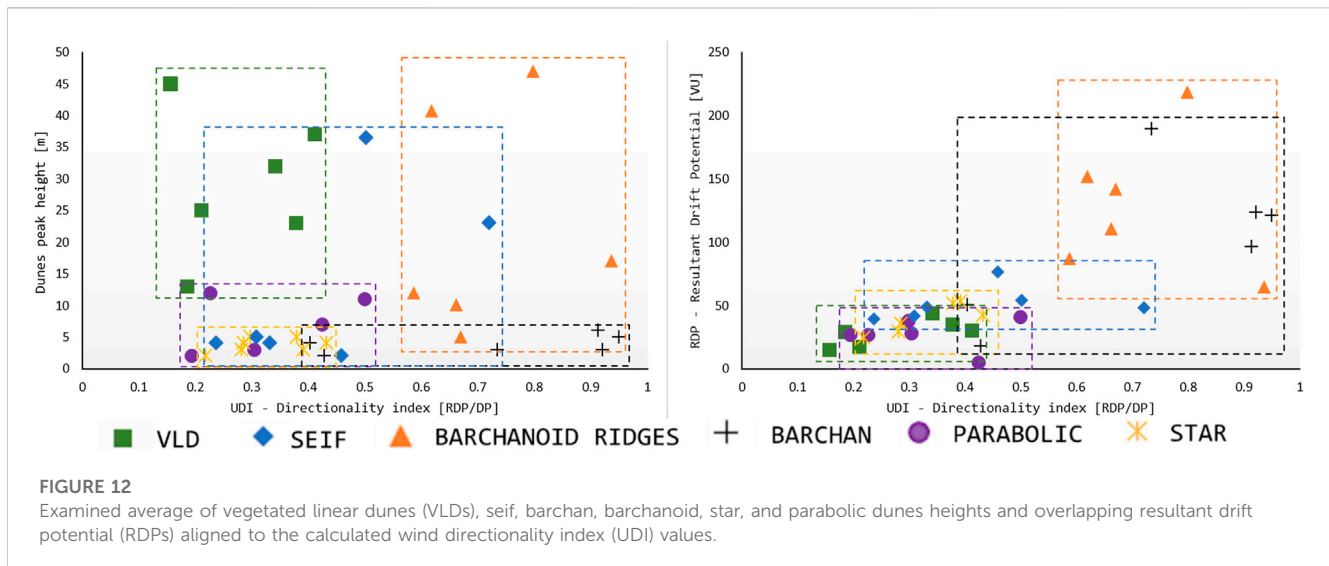


FIGURE 11 Dune types recognized in the area and their drift potential (DP) calculations for the statistical period 2010–2019. The number in the upper left corner stands for the corresponding window in Figure 2. The Coastal Caspian region is split into Northern Hemisphere seasons, winter (November–February) and summer (May–August), as well as the geomagnetic time hour of sampling of the reanalysis data, 06:00 h and 18:00 h, for 2010–2019.

reworking of the VLD crest lines in both the Karakum and Kyzylkum deserts, with the RDP values being less than 50 VU. Under the current unimodal wind regime, the latest eastern section of the Kyzylkum Desert exposes stable VLDs, where the RDP values are extremely low and the RDD is almost perpendicular to the longitudinal axes of the dunes. As VLDs appear considerably larger than the power of the present erosive winds, this underlies their certain genesis during times of significantly stronger winds with somewhat uni- to bi-modal regional wind directions (Wasson and Hyde, 1983; Craddock et al., 2015) and drastically higher availability of sand supply (Maman et al., 2021).

The area’s second dominant structures were large barchanoid ridges on the Caspian Sea shore, with the crest lines being aligned N-S and the typical height being 30–50 m. Their stoss slopes were superimposed by seif dunes that were primarily oriented ENE–WSW, with clean interdunal areas that were seasonally filled with water. Compared to the underlying barchanoid ridges, the overlaid forms of the seif dunes were correlated with the predicted annual RDDs. Overall, the barchanoid ridges identified in the study area were altered by moderate (0.6) to uni- (0.95) directional winds, with the RDPs ranging from 50 VU to 300 VU, the highest discovered RDPs in the KKCAD (according to the ERA5 wind reanalysis model).



A large field of barchanoid ridges was recognized in the southern internal area of the Karakum desert, entirely occupied by vegetation and biogenic crusts (Figure 11; inset 11). Although the annual RDD correlated with the orientation of the barchanoid crest lines, the RDP revealed extremely low values of nearly 15 VU, indicating that the area supports vegetation growth and crust development. Altogether, this area received an average annual precipitation of more than 125 mm over the previous four climatic cycles, with moderate drifting wind velocities maintaining the sturdiness of these barchanoid ridges, in contrast to those recorded on the coast. Furthermore, simple barchans were observed along both sides of the Amu-Darya River. The height of the simple barchans in the KKCAD is not more than 10 m, and the dunes are aligned to their sizes by multi (RDP/DP ~ 0.4) to uni (RDP/DP ~ 0.96) directional winds, with RDP values of 10–200 VU, as observed in the Karakum and Kyzylkum deserts.

The seif and star dunes generally appear together as fully active formations in the KKCAD, although they comprise a minor area, compared to the previously discussed aeolian arrangements. In this study, the seif dunes were oriented NE–SW in the surveyed areas and were highly aligned with the calculated RDDs. They were registered in active patches in the dipper desert and in complex and compound settings on the Caspian shore, where they overlapped giant barchanoid ridges and other, larger, seif formations, respectively. At the top of the giant barchanoid dunes, seif dunes result from the bed instability of the underlying barchan sands (Hu et al., 2021). The directionality index for their formation was 0.5 on average, which accounted for the bi-modal wind regimes expected for their formation. The height of the seif dunes observed in the Karakum and Kyzylkum was 5–30 m, formed when the RDP values were roughly 40–100 VU. The star dunes were the rarest dune types recognized in the study area. They occupied a small region in South Kyzylkum at the Amu-Darya River and coexisted in active patches, together with transverse and seif dunes. Although the star dunes were a minority in the study region, when looking at high-resolution images, we observed that blended with the seif dunes, they override the discussed coastal barchanoid ridges. Their heights did not exceed 10 m, and their

formation was followed by RDPs of less than 60 VU for conditions of multi-to-moderate wind variability ($0.2 < \text{RDP/DP} < 0.45$).

Parabolic dunes were observed to have small (3 m) to medium (12 m) heights. As these dunes were noticeably smaller than other formations (same represented star dunes and seif dunes), because of the insufficient DEM resolution, their actual sizes may differ in nature. In the study area, they exist in conditions of high to moderate wind variability ($0.2 < \text{RDP/DP} < 0.5$) and with low RDP values that did not exceed 50 VU. Recognized forms have a U-shape over the entire observed region without exhibiting a V shape. According to multi-spectral satellite imagery, dunes in the area certainly demonstrate a trend of the south–north imposition. Such orientation is not in line with the present RDD route in the region. The dunes were interspersed with circularly arranged cavities in the sand, along with circular arrangements of vegetation in the extended portion of the region, possibly explained as either a honeycomb formation or a massive manifestation of internal old and complex blowout dunes scooped out by the wind (discussed in further text).

Although the active patches in internal KKCAD revealed the presence of additional transverse and star dune blends, they represented a minority that could not be studied using the current satellite data, due to the poor resolution of the existing models, as noticed for parabolic dunes.

4.2.2 Uncertain dune types

Two forms of parabolic-like formations have been identified that cannot be linked to recognized behaviors of parabolic dunes in general (Figure 13). Honeycomb-like dunes formations were found in various locations south of the Sarygamysh Lake and Aral sea, where they portrayed a complex of vegetated and crusted settings. According to Jakel (2004), a honeycomb dune is formed on dune slopes in active dune fields because of the sand's reaction to rain and wind. Following a rain event, the wind uncovers and removes the dry sand beneath the wet layer, producing holes up to 0.5 m in depth and causing the wet sand to sink. This movement exposes dry sand, whereas continual rain prevents further deflation. The same processes can occur on the crests of the dunes. Conversely,

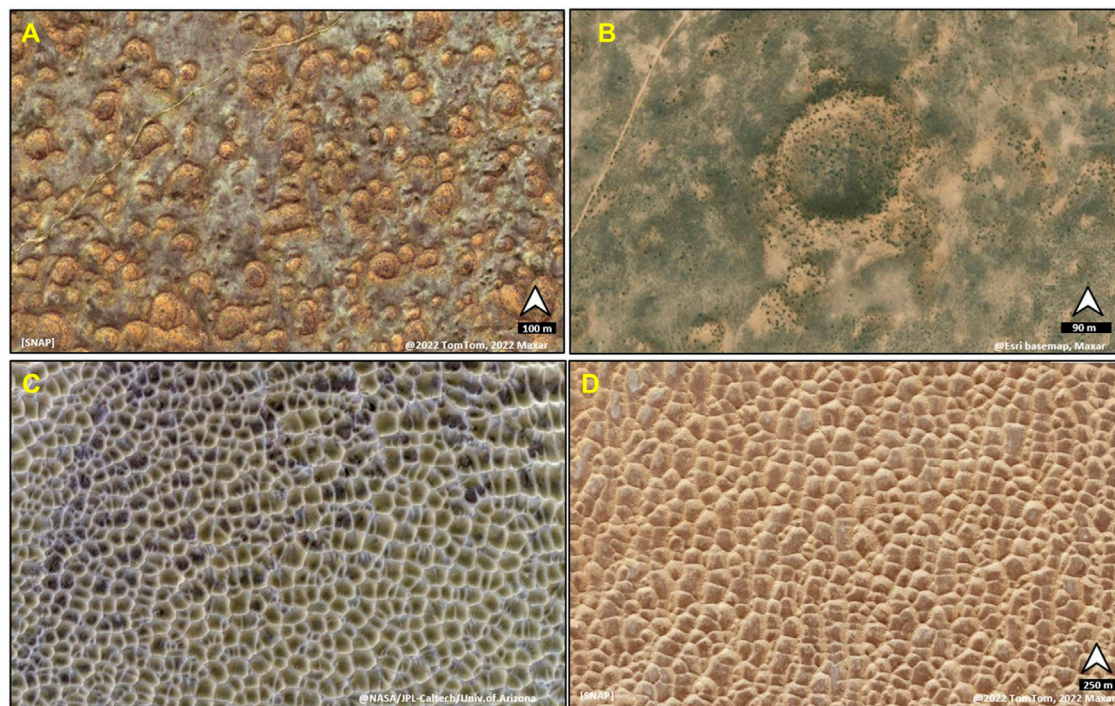


FIGURE 13

Uncertain dune types. (A) bowl-like formations snapped from ©Bing Maps Aerial Imagery and adapted. (B) Fully stabilized bowl-like form, with partially vegetated bounding ring and adapted from Esri (C) Martian honeycomb dunes, taken from NASA official webpage (D) Karakum honeycomb pattern snapped from ©Bing Maps Aerial Imagery and adapted.

honeycomb dunes have been identified as permanent and semi-fixed sand dunes in the Chinese deserts by Zhenda and Youlin (1990) and Liu et al. (2015).

Northern of the Aydakul Lake, in variety of sizes, vegetated linear bowl-shaped formations are recognized. They were seen as spatially exceptionally dense (Figure 13). With the yearly average precipitation ranging from 150 mm (minimum) to 400 mm (maximum) during the preceding four climatic cycles, the vast field of bowl-like dunes observed in the eastern Kyzylkum region was also the region with the highest average annual precipitation. This explained the extensive distribution of biogenic crusts and vegetation over the eastern region. Except in the eastern Kyzylkum, a described unique behavior was not recognized in other places of KKCAD.

Notably, blowout dunes are commonly described as the place of origin of U-shaped parabolic dunes (Livingstone and Andre, 1996) and/or a common feature superimposed on a parabolic formation (Hesp et al., 2016; Tripaldi et al., 2018), referring to superimpositions on mega-dunes. They can be correlated to biotic and abiotic developmental processes, such as vegetation-induced blowout closure and erosional blowout expansion, respectively (Schwarz et al., 2018). According to Smyth et al. (2020), erosional hollows in dunes are essential natural processes for landscape disturbance, because they break the succession of the dune and provide a supply of nutrient-deficient sand *via* aeolian (wind) sediment erosion and the subsequent deposition. Generally, such forms were recorded in coastal regions (Sloss et al., 2012;

Schwarz et al., 2018), although a recent assessment by Tripaldi et al. (2018) depicted the existence of blowouts in giant parabolic dunes found in Argentina's inland subtropical dune fields. Nonetheless, most of the investigated bowl-like formations in the KKCAD do not include active sand; rather, their core bodies are wholly or partially stabilized by the crust, distinguishing them from the reported coastal blowouts.

Thus, in this study, we questioned two different formations: the honeycomb form, which is more consistent with the phenomenon observed in the western KKCAD region around the lakes, and the bowl-like-form, observed in the eastern region of the Kyzylkum. Their relation to contemporary winds is unclear, as it is unknown which climatic and environmental setting is required for their initiation, retention, or maintenance. Notably, the important question that arises from this observation is whether these bowl-shaped dunes represent paleo-blowouts or a new type of sand dune formation. Due to the lack of better resolution of the currently available DEMs and the inability to conduct or compare the field examinations of mentioned formations in the KKCAD area or the Central Asian region (due to the short timeframe of the ongoing project), it remains hypothetical whether the circular pattern recognized in the eastern Kyzylkum Desert represents a novel dune kind. Honeycomb dunes are mentioned but not examined in the literature on aeolian structures; consequently, the mapping and morphological understanding of the "honeycomb" structure remains unclear.

5 Discussion

5.1 Dunes morphologies and environmental system dynamics

The dynamic evolution of various dunes in a sand sea is a complex process that includes different elements, ranging from local topography, sand transport, wind performances, and energy exchange (Bagnold, 1941; Pye and Tsoar, 2009; Charru et al., 2013; Hu et al., 2021; Gadal et al., 2022) to a complex sequence of interactions between different morphologies, anthropogenic disturbances and various plant cover rates (Gao et al., 2015; Hu et al., 2021). Although some of these components may be predicted and modeled effectively, other environmental and anthropogenic factors may be more difficult to model. In particular, wind regime and sand availability have an impact on dune morphologies, especially bedforms (Wasson & Hyde, 1983; Cooke et al., 1993; Courrech du Pont et al., 2014; Gao et al., 2015), and their spatial pattern is largely governed by the history of these two variables (Reffet et al., 2010; Pye et al., 2019; Hu et al., 2021). In recent years, more attention has been given to model relationship between stabilization agents and effect of plants and biogenic crust on dunes morphodynamics (e.g., Kinast et al., 2013; Chen et al., 2021; Gadal et al., 2022).

The diversity of the Central Asian landscape and climate, in general, is widely acknowledged (e.g., Shahgedanova, 2003; Dallmeyer et al., 2010; Cheng et al., 2016), especially as an arid-marginal region subjected to rapid land-use changes and desertification processes (Lioubimtseva et al., 2005; Lioubimtseva and Cole, 2006; Lioubimtseva, 2015; Pueppke et al., 2018); however, for the KKCAD region, the nature of the interaction between the desert land surface forms and the atmosphere is poorly understood and underestimated in the existing literature. Even though the relationship between aeolian morphology and wind regimes is complicated by the presence of relict forms (Wilson, 1973; Maman et al., 2011), the sediment availability, underlying local topography (Wasson and Hyde, 1983), the interplay between synoptic-scale airflow and high mountain belts (Fitzsimmons et al., 2020), northerly and easterly winds are still evident in KKCAD. Notably, vegetation and biogenic crust communities represent a distinct factor that additionally modulates and weakens their present reworking of the sandy deserts. In this assessment, we observed that the bulk of the examined aeolian formations in the study area was stable, including the active zone that was not devoid of sparse vegetation or vegetation-crust blends that do not interfere with the operation of the dunes or results in semi-stabilized sands, as commented by Maman et al. (2011). Because of the high precipitation rate during the past 120 years (150–400 mm/yr), in a gradient from west to east, low wind-drift potential ($DP < 100VU$) and moderate wind regime ($RDP/DP \sim 0.4$), the growth of vegetation and biogenic crusts improved (Ashkenazy et al., 2011; Maman et al., 2011) in the entire region. Once established, they will most likely provide long-term stability to the underlying aeolian arrangements (Neuman and Maxwell, 1999; Argaman et al., 2006; Ashkenazy et al., 2011; Maman et al., 2011). This is further supported by climate change studies and the scenarios of the interaction between biogenic crust with the available CO_2 in the atmosphere (Ashkenazy et al., 2011). In KKCAD, such

scenario coincides with the report of Lioubimtseva et al. (2005) on the increased proliferation of biogenic crusts over the past several decades in the Karakum Desert, as the crust consumes CO_2 to flourish. Previous studies have shown that the crust, composed of cyanobacteria, algae, lichen, and mosses, is not a rare formation in the world's sand seas (Maman et al., 2011), and a distinct feature of the main sand seas is the presence of considerable regions of stabilized dunes on their margins, most of which were active during the last glacial maximum (LGM) (Sarnthein, 1978; Sarnthein et al., 1981; Pye and Tsoar, 2009). For example, both the Kalahari Basin and Australian dunes are covered with biogenic, primarily cyanobacterial crusts (Hesse and Simpson, 2006; Thomas and Dougill, 2006; 2007; Ashkenazy et al., 2011), that are most likely to be further developed and impacted by changes in the future climate. As the Karakum and Kyzylkum deserts are dominated by both vegetation and crusts, which blanket dominant NNW-SSE and N-S trends of dunes, the emergence of active patches determined in randomly isolated and stable locations is unknown and has previously been questioned by Maman et al. (2011). One of the assumptions is that crust was eroded from fully stabilized sandy lands creating active patches as a result. According to Ashkenazy et al. (2011), biogenic crusts can withstand strong winds (up to 30 m/s), without experiencing erosion (Neuman and Maxwell, 1999; Argaman et al., 2006), survive in a dormant mode in drought conditions, and return to active growth and development within a few hours after rainfall (even if the precipitation is low). Still, the type of driving climatic forces that can erode a biogenic crust and lead to the reactivation of dunes remains unclear. New studies on dunes bistability suggests different mechanisms for active-stable dunes coexistence in the same geographic area where phenomenon cannot be explained using hysteresis curve theory (Tsoar, 2005), discussed further in the text.

5.2 Climate and paleoclimate intersects

The aeolian sand and loess deposition in KKCAD suggest the increase in the strength and intensity of wind activity during the LGM, which boosted the aeolian transport and the formation of mega aeolian dunes (Maman et al., 2021). Previous studies have proposed that the Mid-Holocene transition from dry and cold to more humid and warm conditions, with low wind power (McGee et al., 2010), led to changes in the current landscapes of Central Asia, and thus the Karakum and Kyzylkum sand seas. Dodonov and Baiguzina (1995) suggested a model centered on the glacial-interglacial cyclicity of the Asiatic high (Siberian-Mongolian) and the westerlies during the Pleistocene period. According to Maman et al. (2021), cold winds flowed from the Northern European ice sheet to the south during glacial eras, which may explain the current dune direction in the study area. As the wind force was not adequate to produce sand movement or inhibit plant germination, even during the Mid-Holocene, dune stabilization was initiated in the region. Furthermore, the wetter environment and greater precipitation promoted vegetation and the production of biogenic crusts (Maman et al., 2011), which helped stabilize the dunes (Kidron et al., 2010). Studies on the lake sediments in Central Asia demonstrated a considerable rise in the effective moisture content between 8 ka and 4 ka during the mid-Holocene period

(Chen et al., 2008; Rudaya et al., 2009). The OSL dates reported by Maman et al. (2021) did not match the clusters of sand-deposition ages reported in other studies (Li et al., 2002; Zhou et al., 2008; He et al., 2010; Roskin et al., 2011b; Li and Fan, 2011; Fitzsimmons et al., 2020), that indicated the initiation of dune stability during the Early or Late Holocene period. Fitzsimmons et al. (2020) reported only one OSL date for the Moyunkum Desert (southern Kazakhstan), which is consistent with the period of dune activity in the KKCAD. The longitudinal axes of the linear dunes reported in the western section of Moyunkum were generally oriented north-south, trending somewhat to the east, which corresponded to the orientation of the VLDs observed in the KKCAD region. Thus, we could conclude that the climate of the Moyunkum desert, north-east of the KKCAD, was and is virtually the same as that responsible for the dune formation and activity in the KKCAD. Compared to our study, dunes in Khartouran Erg (northeastern Iran) revealed similar wind performances. There, erosive winds are indicative of a low-energy environment (Rahdari and Rodríguez-Sejjo, 2021) and predominantly enter from the eastern and northern directions with a directionality index ranging between 0.3 and 0.6. While wind-carried sand has a southwest trajectory, authors suggest that sand dunes have been fixed for a long time historically. Such observation coincides with our results for the KKCAD region. In contrast, in the Registan sand sea (southwestern Afghanistan), the present climatic conditions differ drastically and represent unimodal wind regimes, presently reworking barchanoid dunes of different sizes along the region (Abbasi et al., 2018).

Finally, the great majority of the KKCAD is represented by complex and compound linear forms, stabilized by blends of vegetation and biogenic crusts. Where dunes are seen as active, they rarely appear in simple forms and are usually superimposed on top of other linear or barchanoid dunes. In contrast to extremely complex stable formations, the mechanism for active dunes formation is known and in line with calculated drift potentials and general wind interactions with active linear profiles. Other active forms identified in the area stand for barchans and barchanoid ridges, with the exception of discussed stabilized barchanoid field in Karakum desert. Thus, the Karakum and Kyzylkum deserts are accepted as relicts of a former sand sea.

When it comes to previously discussed active-stable dunes coexistence, a recent study by Xu et al. (2020) showed different paths of recovery and collapse of vegetation at system-wide scales, implying that hysteretic behavior occurs in spatially extended systems which supports co-existence of active and stable dune fields in small proximities. They suggested that the exact timing of changes in dune state at individual sites can be determined by numerical dating (e.g., OSL dating technique) and that a careful site-specific reconstruction of temporal changes in dune activity at individual sites or the cluster of multiple well-dated dune records will reveal the temporal pattern of dune field activity during the past 12,000 years and substantial differences in dune state shifts between individual sites. In that regard, studies on biogenic soil crusts in Central Asia are generally limited (Büdel, 2001) and only a few sites are well-documented and dated (Chandler, 2015; Pye et al., 2019; Hu et al., 2021; Maman et al., 2021), thus precise conclusion on shifts between states of stability of dunes in KKCAD requires precise and careful field assessments and modeling. This hinders our ability to

derive precise links and discuss temporal variations between the present and paleo-wind characteristics in active zones of KKCAD and determine the eventual periods of patch reactivations at individual sites.

5.2.1 Aeolian-fluvial interactions

As it splits two sand seas, the Amu-Darya is assumed to be the most important river and agent in aeolian-fluvial interactions for the KKCAD region. The local name of the Amu-Darya River is “Jeikhun” or “mad”, which is explained by river’s dynamical nature throughout history, as well as its ability to shift and modify its course and destroy riverbanks in sudden events. According to Berkovich et al. (1973), in 1898 in the upstream near Kerki town, Amu-Darya washed 10 m of the riverbank for 6 min, followed by an event in 1932 when it washed 500 m of the bank near Turtkul town. Amu-Darya River is characterized by low bed stability and a very large volume of sediments. One of the important factors specific to the Amu-Darya is a decrease of sediment volume downstream as a result of their accumulation, which causes systematic increase of the bottom of the channel (Berkovich et al., 1973) and may influence processes around, as river splits two sand seas. Separate sandy ridges, stretched along the dominant direction of the wind, move from the terrace to the floodplain, crossing the curved shapes of the manned floodplain relief. Barchans invade the left bank floodplain, descending from the watershed plateau (Chalov, 2022).

Maman et al. (2021) reported that most of the sand samples collected for OSL measurements, showed unimodal distributions typical of aeolian sand and are classified as fine to very fine sands. All samples displayed positive skewness values indicating that the distribution has a more pronounced tail of fine material compared with a log-normal distribution (Pye and Tsoar, 2009), which corresponds to dune sand and river sand sources that are positively skewed (Besler, 2008). Sand samples taken in the eastern sands of KKCAD were well to moderately well sorted with values lower than or close to unity, while the western samples were moderately to very poorly sorted (Maman et al., 2021), which may be attributed to their relative proximity to the source of the sand (Pye and Tsoar, 2009), the Amu-Darya River that drains the Pamir mountains.

Petrov (1976) described the KKCAD as alluvium-aeolian sands. Tectonic activity in the Central Asian area decreased throughout the Quaternary when alluvial deposits were modified by aeolian activity (Atamuradov, 1994). According to Atamuradov (1994), the area’s climate alternated between humid and arid during the Quaternary, and the level of the Caspian Sea fluctuated as well, affecting the course of the Amu-Darya River when aeolian bedforms emerged.

Study of the transition from dune environment to the fluvial dominated environment in the Negev Desert in Pleistocene-early Holocene showed the sensitivity of sandy river margins to the alternation of aeolian-fluvial processes. Aeolian domination occurs when wind power increases, while increasing fluvial activity under humid conditions of early-Holocene, led to sedimentation in water bodies (Robins et al., 2022). Thus, it can be assumed that active dunes—times of aeolian domination blocked watercourses in the KKCAD while stabilization times, lead to a return to fluvial domination at present days.

5.3 Unique dune types in the region

The parabolic bowl-shaped dunes seen in satellite imagery and referred to as “parabolic” by Maman et al. (2021) differ from the information of such dunes in other regions, especially when using high-resolution data. Notably, in this study, these dunes were almost evenly spread over an area that exceeded 30,000 km², with the diameter ranging from 30 to 300 m (average), portraying a distinct vegetated perimeter (in the form of a bounding ring), without a flat surface in the center (Figure 13). They may represent some revered forms of parabolic dunes, reworked by the generation of winds and currently stabilized by the contemporary ones. These structures registered in eastern Kyzylkum must be further analyzed in field data acquisition, in order to explore their potential linkage to the existing aeolian literature or announce them as novel.

As no detailed geomorphological studies of honeycomb dunes on the Earth have been identified, we find these bedforms to be extremely interesting, analogous to the honeycomb dunes observed by the National Aeronautics and Space Administration (NASA) Mars Reconnaissance Orbiter High Resolution Imaging Science Experiment (HiRISE)⁶. Their patterns have been compared with those identified in the KKCAD region (Figure 13). However, the Martian dune fields seem to represent active aeolian forms, whereas stabilized and predominantly crusted, and somewhat partially active forms, were observed in the KKCAD region in this study. Note that NASA suggests that this type of dune form does not originate as wind-blown dunes, interpreting the polygons as evidence of a dried-up lake⁷. As the honeycomb pattern is seen further south in regions of the Sarygamish Lake and the Aral Sea, we could conclude that the same environmental mechanism could be responsible for their development on the Earth. Similar reticulated structures identified in different areas on Mars are termed “networking dunes”, although mentioned structures are considered there as complex star formations, or some form of reversing transverse dunes, formed by the stronger multidirectional winds (Keszthelyi et al., 2008; Kerber & Head, 2011; Hargitai, 2014). It could be suggested that existence and geomorphological appearance of these dunes structures on Mars should be examined in relation to present and paleo aeolian forms and climatic performances on Earth (e.g., those discussed for KKCAD).

6 Conclusion

To evaluate the winds in the region, their necessary forces and trajectories to produce sand germination and support present alignment to the underlying dune orientation, we utilized the processing and fusion of numerous different forms of data types, statistical processing methods, GIS analysis, and satellite imaging observations.

The crucial phase addressed by this study was the performance assessment of both the data sources, as the majority of current aeolian studies concerning wind spatiotemporal performances in the world’s deserts either apply the wind data derived from discrete locations (weather stations) or from reanalysis models. Reanalysis

models are known to exaggerate or underestimate wind speeds. However, for this site, we chose the ERA5 dataset as a more credible wind data source, as it offers an alignment between the estimated RDDs and orientation of active morphologies.

Through multidimensional raster analysis, we present a novel method for examining the drift potential of aeolian deserts. Apart from shoreline and takyr area, the calculated DP values over the KKCAD region portray a predominately negative trend of change over the previous 7 decades, suggesting that these sand seas will eventually entirely stabilize. Throughout the same statistical period, 93% of the region was part of a low-energy environment (<200 VU).

The morphological categorization of the dune types in the KKCAD revealed a complex mosaic of dunes of various forms and generations. Such complexity develops because dunes of various sizes respond to changing wind patterns at varying speeds, resulting in morphologies that symbolize the integration of partial geomorphological adjustment to a plethora of past wind occurrences (Pye et al., 2019; Hu et al., 2021). The strength of the present wind that flows from the North and Northeast directions in the Central Asian deserts is substantially lower than that of the historic prevailing winds, resulting in the stability of the region’s massive aeolian morphologies. Thus, the dune shape, orientation, level of complexity, and various levels of bed stability in the Karakum and Kyzylkum deserts suggest that several dune generations evolved through a series of rework and stabilization of older sands.

This study explored the novel dune types identified in the study area that could not be related to the existing aeolian literature on active and stable aeolian dune forms. With minor exceptions in the study region, we demonstrated that the dunes in the Karakum and Kyzylkum regions exhibit distinctive characteristics reminiscent of relict environments. We conclude that the current alignment of dune orientations, with the calculated resultant drift directions and powers, should be further examined in relation to paleoenvironmental conditions and additional OSL dating, at a sufficient spatial resolution, applicable to the large extent of the KKCAD. The dynamics of the contemporary stabilization could be eventually assessed, by tracking the dynamics of the biogenic crusts and the anthropogenic/environmental disturbances, which for areas of vast extents, such as sand seas, can be carried out using satellite imagery, time-series analysis and machine or deep learning modeling. Furthermore, we suggest that multidimensional data mining methods applied in this study can be used to analyze the relationship between aeolian geomorphology and climate in other arid or non-arid world regions.

Data availability statement

The original contributions presented in the study are included in the article/Supplementary Material, further inquiries can be directed to the corresponding author.

Author contributions

MP: Conceptualization, Formal analysis, Investigation, Software, Visualization, Writing–Original Draft DB: Validation, Supervision, Funding acquisition, Writing–Review and Editing LO: Validation,

6 URL: <https://mars.nasa.gov/resources/7143/polygonal-sand-dunes>

7 URL: <https://mars.nasa.gov/>

Supervision, Funding acquisition, Writing–Review and Editing SM: Conceptualization, Validation, Resources, Supervision, Project administration, Funding acquisition, Writing–Review and Editing

Funding

This research was supported by the Israel Science Foundation through grant 1030/21, we gratefully acknowledge this support.

Acknowledgments

We would like to thank Dr Aviv-Cohen Zada for providing his assistance in the sand rose calculations and Prof. Haim Tsoar for his insightful comments.

References

- Abbasi, H., Opp, C., Groll, M., and Gohardoust, A. (2019). Wind regime and sand transport in the Sistan and Registan regions (Iran/Afghanistan). *Z. für Geomorphol. Suppl. Issue* 62, 41–57. doi:10.1127/zfg_suppl/2019/0543
- Abdrakhmatov, K. Y., Aldazhanov, S. A., Hager, B. H., Hamburger, M. W., Herring, T. A., Kalabaev, K. B., et al. (1996). Relatively recent construction of the Tien Shan inferred from GPS measurements of present-day crustal deformation rates. *Nature* 384, 450–453. doi:10.1038/384450a0
- Argaman, E., Singer, A., and Tsoar, H. (2006). Erodibility of some crust forming soils/sediments from the Southern Aral Sea Basin as determined in a wind tunnel. *Earth Surf. Process. Landf.* 31, 47–63. doi:10.1002/esp.1230
- Ashkenazy, Y., Yizhaq, H., and Tsoar, H. (2011). Sand dune mobility under climate change in the Kalahari and Australian Deserts. *Clim. Change* 112, 901–923. doi:10.1007/s10584-011-0264-9
- Atamuradov, K. I. (1994). “Paleogeography of Turkmenistan,” in *Biogeography and ecology of Turkmenistan*. Editors V. Fet and K. I. Atamuradov (Dordrecht: Kluwer Academic Publishers), 49–64.
- Babaev, A. G. (1994). “Landscapes of Turkmenistan,”. Editors V. Fet and K. I. Atamuradov (Dordrecht: Kluwer Academic Publishers), 5–22. *Biogeography and Ecology of Turkmenistan Partial*
- Babaev, A. G. (1972). Physical geography of Turkmenistan. *Geology of the USSR. Turkm. SSR* 22, 22–31.
- Bagnold, R. A. (1941). *The physics of blown sand and desert dunes*. London, UK: Methuen and Co.
- Berkovich, K. M., Lodina, R., and Chalov, R. (1973). Solid sediments and patterns of channel deformations in the upper reaches of the Amuarya. *Soil Eros. channel Process.* 3, 241–262.
- Besler, H. (2008). *The great sand sea in Egypt: Formation, dynamics and environmental change-a sediment-analytical approach*. Elsevier Science.
- Breed, C. S., Fryberger, S. G., Andrews, S., McCauley, C., Lennartz, F., Gebel, D., et al. (1979). Regional studies of sand seas using Landsat (ERTS) imagery. *A Study Glob. Sand Seas*. 1052, 305–398.
- Büdel, B. (2001)., 150. Berlin, Germany: Springer, 141–152. Synopsis: Comparative biogeography of soil-crust biota *Ecol. Stud.*
- Caves, J. K., Moragne, D. Y., Ibarra, D. E., Bayshashov, B. U., Gao, Y., Jones, M. M., et al. (2016). The neogene de-greening of central Asia. *Geology* 44 (11), 887–890. doi:10.1130/G38267.1
- Chalov, R. S. (2022). Influence of aeolian processes (wind factor) on the formation and morphology of channels and floodplains of plain rivers. *Phys. Geogr. Landscapes Geomorphol.*, 7–16. doi:10.17072/2079-7877-2022-2-6-16
- Chandler, C. K. (2015). *Superimposed and auxiliary dunes of the northern Namib sand sea: A ground-penetrating radar study*. Provo, UT: Brigham Young University.
- Charru, F., Andreotti, B., and Claudin, P. (2013). Sand ripples and dunes. *Annu. Rev. Fluid Mech.* 45, 469–493. doi:10.1146/annurev-fluid-011212-140806
- Chen, Y., Yu, Z., Yang, M., Ito, E., Wang, S., Madsen, D. B., et al. (2008). Holocene moisture evolution in arid central Asia and its out-of-phase relationship with Asian monsoon history. *Quat. Sci. Rev.* 27, 351–364. doi:10.1016/j.quascirev.2007.10.017
- Chen, Y., Yizhaq, H., Mason, J. A., Zhang, X., and Xu, Z. (2021). Dune bistability identified by remote sensing in a semi-arid dune field of northern China. *Aeolian Res.* 53, 100751. doi:10.1016/j.aeolia.2021.100751
- Cheng, H., Spötl, C., Breitenbach, S. F. M., Sinha, A., Wassenburg, J. A., Jochum, K. P., et al. (2016). Climate variations of Central Asia on orbital to millennial timescales. *Sci. Rep.* 6, 36975. doi:10.1038/srep36975
- Climate Change Knowledge Portal (Cckp) (2021). *Metadata*.
- Cohen-Zada, A. L., Maman, S., and Blumberg, D. G. (2017). Earth aeolian wind streaks: Comparison to wind data from model and stations. *J. Geophys. Res. Planets* 122, 1119–1137. doi:10.1002/2016JE005242
- Cooke, R. U., Warren, A., and Goudie, A. S. (1993). *Desert geomorphology*. London, UK: CRC Press.
- Courrech du Pont, S., Narteau, C., and Gao, X. (2014). Two modes for dune orientation. *Geology* 42, 743–746. doi:10.1130/G35657.1
- Craddock, R. A., Tooth, S., Zimbelman, J. R., Wilson, S. A., Maxwell, T. A., and Kling, C. (2015). Temporal observations of a linear sand dune in the Simpson Desert, central Australia: Testing models for dune formation on planetary surfaces. *J. Geophys. Res. Planet* 120, 1736–1750. doi:10.1002/2015JE004892
- Dallmeyer, A., Clausen, M., and Otto, J. (2010). Contribution of oceanic and vegetation feedbacks to Holocene climate change in monsoonal Asia. *Clim. Past*. 6, 195–218. doi:10.5194/cp-6-195-2010
- Dettman, D. L., Kohn, M. J., Quade, J., Ryerson, F. J., Ojha, T. P., and Hamidullah, S. (2001). Seasonal stable isotope evidence for a strong Asian monsoon throughout the past 10. *Y. Geol.* 29, 31–34. doi:10.1130/0091-7613(2001)029<0031:SSIEFA<2.0
- Dodonov, A., and Baiguzina, L. (1995). Loess stratigraphy of central Asia: Palaeoclimatic and palaeoenvironmental aspects. *Quat. Sci. Rev.* 14, 707–720. doi:10.1016/0277-3791(95)00054-2
- Dubief, J. (1952). Le vent et le déplacement du sable au Sahara. *Trav. Inst. Rech. Sahar.* 8, 123–162.
- Fitzsimmons, E. K., Nowatzki, M., Dave, A. K., and Harder, H. (2020). Intersections between wind regimes, topography and sediment supply: Perspectives from aeolian landforms in Central Asia. *Palaeogeogr. Palaeoclimatol. Palaeoecol.* 540, 109531. doi:10.1016/j.palaeo.2019.109531
- Franz, H.-J. (1973). *Physische geographie der Sowjetunion*. Gotha, Germany: Haack.
- Fryberger, S. G., and Dean, G. (1979)., 1052. Washington, DC, USA: US Government Printing Office, 137–169. Dune forms and wind regime *A Study Glob. Sand Seas*
- Fryberger, S. G. (1979). “Dune forms and wind regime,” in *A study of global sand seas*. Editor E. D. McKee (Washington, DC, USA: United States Government Printing Office), 137–170.
- Gadal, C., Delorme, P., Narteau, C., Wiggs, G. F., Baddock, M., Nield, J. M., et al. (2022). Local wind regime induced by giant linear dunes: Comparison of ERA5-land reanalysis with surface measurements. *Boundary-Layer Meteorol.* 185 (3), 309–332. doi:10.1007/s10546-022-00733-6
- Gao, X., Narteau, C., Rozier, O., and Courrech du Pont, S. C. (2015). Phase diagrams of dune shape and orientation depending on sand availability. *Sci. Rep.* 5, 14677. doi:10.1038/srep14677

Conflict of interest

The authors declare that the research was conducted in the absence of any commercial or financial relationships that could be construed as a potential conflict of interest.

Publisher's note

All claims expressed in this article are solely those of the authors and do not necessarily represent those of their affiliated organizations, or those of the publisher, the editors and the reviewers. Any product that may be evaluated in this article, or claim that may be made by its manufacturer, is not guaranteed or endorsed by the publisher.

- Getis, A., and Orid, J. K. (1996). in *Local spatial statistics: An overview* in *spatial analysis: Modeling in GIS environment*. Editor P. M. LongelyBatty (New York, NY, USA: John Wiley & Sons Inc.), 261–278.
- Getis, A., and Orid, J. K. (1992). The analysis of spatial association by use of distance statistics. *Geogr. Anal.* 24 (3), 189–206. doi:10.1111/j.1538-4632.1992.tb00261.x
- Hargitai, H. (2014). Dune-field patterns. *Encyclopedia Planet. Landforms* 1–12.
- Harris, I., Osborn, T. J., Jones, P., and Lister, D. (2020). Version 4 of the CRU TS monthly high-resolution gridded multivariate climate dataset. *Sci. Data* 7, 109. doi:10.1038/s41597-020-0453-3
- He, Z., Zhou, J., Lai, Z., Yang, L., Liang, J., Long, H., et al. (2010). Quartz OSL dating of sand dunes of late Pleistocene in the mu us Desert in northern China. *Quat. Geochronol.* 5, 102–106. doi:10.1016/j.quageo.2009.02.011
- Hellwig, A., Voigt, S., Mulch, A., Frisch, K., Bartenstein, A., Pross, J., et al. (2018). Late Oligocene to early Miocene humidity change recorded in terrestrial sequences in the Ili Basin (south-eastern Kazakhstan, Central Asia). *Sedimentology* 65, 517–539. doi:10.1111/sed.12390
- Hesp, P., Smyth, T., Walker, I., Gares, P., and Waskiewicz, T. (2016). Flow within a trough blowout at cape cod. *J. Coast. Res.* 75, 288–292. doi:10.2112/SI75-058.1
- Hesse, P. P., and Simpson, R. L. (2006). Variable vegetation cover and episodic sand movement on longitudinal desert sand dunes. *Geomorphology* 81, 276–291. doi:10.1016/j.geomorph.2006.04.012
- Hu, Z., Gao, X., Lei, J., and Zhou, N. (2021). Geomorphology of aeolian dunes in the Western Sahara desert. *Geomorphology* 392, 107916. doi:10.1016/j.geomorph.2021.107916
- Illenberger, W. K. (1988). The dunes of the alexandria coastal dunefield, alga bay, south Africa. *S. Afr. J. Geol.* 91, 381–390.
- Inman, D. L., Ewing, G. C., and Corliss, J. B. (1966). Coastal sand dunes of guerra negro, baja California, Mexico. *Bull. Geol. Soc. Am.* 77, 787–802. doi:10.1130/0016-7606%281966%2977%5B787%3ACSDOGN%5D2.0.CO%3B2
- Jakel, D. (2004). Initial stages of complex duneforms after rainfall and formation processes of Honeycomb and Kettle dunes in the Badain Jaran Desert (Shamo) in China. *Z. für Geomorphol.* 133, 107–128.
- Jumashov, A. P. (1999). “Genetic types of deserts in central Asia,” in *Desert problems and desertification in central Asia: The researches of the desert institute*. Editor A. G. Babaev (Berlin, Germany: Springer), 77–87.
- Kaufman, L., and Rousseau, P. J. (2009). *Finding groups in data: An introduction to cluster analysis*, 344. John Wiley & Sons.
- Kendall, M. G. (1975). *Rankcorrelation methods*. London, UK: Griffin.
- Kerber, L., and Head, J. W. (2011). A progression of induration in medusae fossae formation transverse aeolian ridges: Evidence for ancient aeolian bedforms and extensive reworking. *Earth Surf. Process. Landf.* 37 (4), 422–433. doi:10.1002/esp.2259
- Keszthelyi, K., Jaeger, W., McEwen, A., Tornabene, L., Beyer, R. A., Dundas, C., et al. (2008). High resolution imaging science experiment (HiRISE) images of volcanic terrains from the first 6 months of the Mars reconnaissance orbiter primary science phase. *J. Geophys. Res. Planets* 113 (E4), E04005. doi:10.1029/2007je002968
- Kidron, G. J., Vonshak, A., Dor, I., Barinova, S., and Abeliovich, A. (2010). Properties and spatial distribution of microbiotic crusts in the Negev Desert, Israel. *Catena* 82 (2), 92–101. doi:10.1016/j.catena.2010.05.006
- Kinast, S., Meron, E., Yizhaq, H., and Ashkenazy, Y. (2013). Biogenic crust dynamics on sand dunes. *Phys. Rev. E* 87 (2-1), 020701. doi:10.1103/PhysRevE.87.020701
- Lancaster, N. (1983). *Developments in sedimentology*. Elsevier, 261–289. doi:10.1016/S0070-4571(08)70799-4Controls of dune morphology in the Namib sand sea
- Lancaster, N. (1995). *Geomorphology of desert dunes*. London, UK: Routledge.
- Lancaster, N. (1989). *The Namib sand sea: Dune forms, processes and sediments*. Rotterdam: Balkema.
- Leighton, C. L., Bailey, R. M., and Thomas, D. S. (2013). The utility of desert sand dunes as Quaternary chronostratigraphic archives: Evidence from the northeast Rub’al Khali. *Quat. Sci. Rev.* 78, 303–318. doi:10.1016/j.quascirev.2013.04.016
- Li, S. H., and Fan, A. (2011). OSL chronology of sand deposits and climate change of last 18 ka in Gurbantunggut Desert, Northwest China. *J. Quat. Sci.* 26, 813–818. doi:10.1002/jqs.1508
- Li, S. H., Sun, J. M., and Zhao, H. (2002). Optical dating of dune sands in the northeastern deserts of China. *Palaeogeogr. Palaeoclimatol. Palaeoecol.* 181, 419–429. doi:10.1016/s0031-0182(01)00443-6
- Li, Y., Song, Y., Fitzsimmons, K. E., Chang, H., Orozbaev, R., and Li, X. (2018). Eolian dust dispersal patterns since the last glacial period in eastern Central Asia: Insights from a loess-paleosol sequence in the Ili Basin. *Clim. Past.* 14, 271–286. doi:10.5194/cp-14-271-2018
- Lindhorst, S., and Reimann, T. (2021). Residual dune ridges: Sedimentary architecture, Genesis, and implications for palaeo-climate reconstructions. *Earth Surf. Process. Landforms* 46 (11), 2177–2194. doi:10.1002/esp.5167
- Lioubimtseva, E. (2015). A multi-scale assessment of human vulnerability to climate change in the Aral Sea basin. *Environ. Earth Sci.* 73, 719–729. doi:10.1007/s12665-014-3104-1
- Lioubimtseva, E., Cole, R., Adams, J. M., and Kapustin, G. (2005). Impacts of climate and landcover changes in arid lands of Central Asia. *J. Arid. Environ.* 62, 285–308. doi:10.1016/j.jaridenv.2004.11.005
- Lioubimtseva, E., and Cole, R. (2006). Uncertainties of climate change in arid environments of Central Asia. *Rev. Fish. Sci.* 14, 29–49. doi:10.1080/10641260500340603
- Liu, B., Jin, H., Sun, L., Sun, Z., and Zhao, S. (2015). Geochemical evidence for Holocene millennial-scale climatic and environmental changes in the south-eastern Mu Us Desert, northern China. *Int. J. Earth Sci.* 104, 1889–1900. doi:10.1007/s00531-015-1161-7
- Livingstone, I., and Andre, W. (1996). *Aeolian geomorphology: An introduction*. Wesley Longman Limited.
- Livingstone, I., Bristow, C., Bryant, R. G., Bullard, J., White, K., Wiggs, G. F. S., et al. (2010). The Namib Sand Sea digital database of aeolian dunes and key forcing variables. *Aeolian Res.* 2, 93–104. doi:10.1016/j.aeolia.2010.08.001
- Lydolph, P. E. (1977). *Climates of the Soviet union*. Elsevier (Elsevier).
- Machalett, B., Oches, E. A., Frechen, M., Zöller, L., Hambach, U., Mavlyanova, N. G., et al. (2008). Aeolian dust dynamics in central Asia during the Pleistocene: Driven by the long-term migration, seasonality, and permanency of the Asiatic polar front. *Geochem Geophys Geosyst.* 9, Q08Q09–10. doi:10.1029/2007GC001938
- Maman, S., Blumberg, D. G., Tsoar, H., Mamedov, B., and Porat, N. (2011). The central asian ergs: A study by remote sensing and geographic information systems. *Aeolian Res.* 3, 353–366. doi:10.1016/j.aeolia.2011.09.001
- Maman, S., Porat, N., Meged, C., Blumberg, D. G., Tsoar, H., Mamedov, B., et al. (2021). in *The Karakum and Kyzylkum sand seas: Linking geomorphology and palaeoclimate* in *Sand dunes of the northern hemisphere: Distribution, formation, migration and management*. Editors L. Qi, M. K. Gaur, and V. R. Squires (CRC Press).
- Mann, H. B. (1945). Nonparametric tests against trend. *Econometrica* 13, 245–259. doi:10.2307/1907187
- McGee, D., Broecker, W. S., and Winckler, G. (2010). Gustiness: The driver of glacial dustiness? *Quat. Sci. Rev.* 29, 2340–2350. doi:10.1016/j.quascirev.2010.06.009
- Mitchell, A. (2005). *Spatial measurements & statistics*. Redlands, CA, USA: ESI Press, 2.The ESRI guide to GIS analysis
- Montero, P., and Vilar, A. J. (2014). TSclust: An R Package for time series clustering. *J. Stat. Soft.* 62 (1), 1–43. doi:10.18637/jss.v062.i01
- Muhs, D. R., and Holliday, V. T. (1995). Evidence of active dune sand on the Great Plains in the 19th century from accounts of early explorers. *Quatern. Res.* 43, 198–208. doi:10.1006/qres.1995.1020
- Neuman, C. M., and Maxwell, C. (1999). A wind tunnel study of the resilience of three fungal crusts to particle abrasion during aeolian sediment transport. *Catena* 38 (2), 151–173. doi:10.1016/s03341-8162(99)00043-0
- Nevodchikova, I. B. (1972). *Characteristics of relief in geology of the USSR*. Turkmen USSR, 681–708.
- Ord, J. K., and Getis, A. (1995). Local spatial autocorrelation statistics: Distributional issues and an application. *Geogr. Ana.* 27, 286–306. doi:10.1111/j.1538-4632.1995.tb00912.x
- Orlovsky, L., Dourikov, M., and Babaev, A. (2004). Temporal dynamics and productivity of biogenic soil crusts in the central Karakum desert, Turkmenistan. *J. Arid. Environ.* 56, 579–601. doi:10.1016/S0140-1963(03)00075-2
- Orlovsky, L., Orlovsky, N., and Durdyev, A. (2005). Dust storms in Turkmenistan. *J. Arid. Environ.* 60, 83–97. doi:10.1016/j.jaridenv.2004.02.008
- Orlovsky, N. (1994). “Climate of Turkmenistan,” in *Biogeography and ecology of Turkmenistan*. Editors V. Fet and K. I. Atamuradov (Dordrecht: Kluwer Academic Publishers), 23–48.
- Owen, L., Fedorovich, B. A., and Babaev, A. G. (2018). “Karakum Desert,” in *Encyclopedia britannica*. <https://www.britannica.com/place/Karakum-Desert>.
- Peeters, A., Zude, M., Kathner, J., Unlu, M., Kanber, R., Hetzroni, A., et al. (2015). Getis–Ord’s hot- and cold-spot statistics as a basis for multivariate spatial clustering of orchard tree data. *Comput. Electron. Agric.* 111, 140–150. doi:10.1016/j.compag.2014.12.011
- Petrov, M. P. (1976). *Deserts of the world*. New York: Wiley.
- Pueppke, S. G., Nurtazin, S. T., Graham, N. A., and Qi, J. (2018). Central asia’s ili river ecosystem as a wicked problem: Unraveling complex interrelationships at the interface of water, energy, and food. *Water* 10, 541. doi:10.3390/w10050541
- Pye, K., Livingstone, I., and Warren, A. (2019). *Global frameworks for aeolian geomorphology: A new introduction*. Oxford: John Wiley & Sons Ltd.
- Pye, K. (1984). *Granular disintegration of gneiss and migmatites*, 12, 191–199. Models of transgressive coastal dune building episodes and their relationship to quaternary sea level changes: A discussion with reference to evidence from eastern australia
- Pye, K., and Tsoar, H. (1990). *Aeolian sand and sand dunes*. London, UK: Unwin Hyman.
- Pye, K., and Tsoar, H. (2009). *Aeolian sand and sand dunes*. Springer Verlag.

- Rahdari, M. R., and Rodríguez-Seijo, A. (2021). Monitoring sand drift potential and sand dune mobility over the last three decades (Khartouran Erg, Sabzevar, NE Iran). *Sustainability* 13, 9050. doi:10.3390/su13169050
- Ruffet, E., Courrech du Pont, S., Hersen, P., and Douady, S. (2010). Formation and stability of transverse and longitudinal sand dunes. *Geology* 38, 491–494. doi:10.1130/G30894.1
- Robins, L., Roskin, J., Yu, L., Bookman, R., and Greenbaum, N. (2022). Aeolian-fluvial processes control landscape evolution along dune field margins of the northwestern Negev (Israel) since the late Quaternary. *Quat. Sci. Rev.*, 107520. doi:10.1016/j.quascirev.2022.107520
- Robins, L., Greenbaum, N., Yu, L., Bookman, R., and Roskin, J. (2021). High-resolution portable-OSL analysis of Vegetated Linear Dune construction in the margins of the northwestern Negev dunefield (Israel) during the late Quaternary. *Aeolian Res.* 50, 100680. doi:10.1016/j.aeolia.2021.100680
- Roskin, J., Blumberg, D. G., and Ktra, I. (2014). Last millennium development and dynamics of vegetated linear dunes inferred from ground-penetrating radar and optically stimulated luminescence ages. *Sedimentology* 61 (5), 1240–1260. doi:10.1111/sed.12099
- Roskin, J., Porat, N., Tsoar, H., Blumberg, D. G., and Zander, A. M. (2011a). Age, origin and climatic controls on vegetated linear dunes in the northwestern Negev Desert (Israel). *Quat. Sci. Rev.* 30, 1649–1674. doi:10.1016/j.quascirev.2011.03.010
- Roskin, J., Tsoar, H., Porat, N., and Blumberg, D. G. (2011b). Palaeoclimate interpretations of Late Pleistocene vegetated linear dune mobilization episodes: Evidence from the northwestern Negev dunefield, Israel. *Quat. Sci. Rev.* 30, 3364–3380. doi:10.1016/j.quascirev.2011.08.014
- Rudaya, N., Tarasov, P., Dorofeyuk, N., Solovieva, N., Kalugin, I., Andreev, A., et al. (2009). Holocene environments and climate in the Mongolian altai reconstructed from the hoton-nur pollen and diatom records: A step towards better understanding climate dynamics in central Asia. *Quat. Sci. Rev.* 28, 540–554. doi:10.1016/j.quascirev.2008.10.013
- Sarnthein, M., Tetzlaaf, M. G., Koopmann, B., Wolter, K., and Pflaumann, U. (1981). Glacial and interglacial wind regimes over the eastern subtropical Atlantic and north-west Africa. *Nature* 293, 193–196. doi:10.1038/293193A0
- Sarnthein, M. (1978). Sand deserts during glacial maximum and climatic optimum. *Nature* 272 (5648), 43–46. doi:10.1038/272043a0
- Schwarz, C., Brinkkemper, J., and Ruessink, G. (2018). Feedbacks between biotic and abiotic processes governing the development of foredune blowouts: A review. *J. Mar. Sci. Eng.* 7, 2. doi:10.3390/jmse7010002
- Shahgedanova, M. (2003). *The physical geography of northern Eurasia*. Oxford University Press on Demand.
- Sloss, C. R., Shepherd, M., and Hesp, P. (2012). Coastal dunes: Geomorphology. *Nat. Educ. Knowl.* 3 (10), 2.
- Smyth, T., Thorpe, E., and Rooney, P. (2020). “Blowout evolution between 1999 and 2015” in *In ainsdale sand dunes national nature reserve, england* (England: North West Geography).
- Thomas, A. D., and Dougill, A. J. (2006). Distribution and characteristics of cyanobacterial soil crusts in the Molopo Basin, South Africa. *J. Arid. Environ.* 64, 270–283. doi:10.1016/j.jaridenv.2005.04.011
- Thomas, A. D., and Dougill, A. J. (2007). Spatial and temporal distribution of cyanobacterial soil crusts in the Kalahari: Implications for soil surface properties. *Geomorphology* 85, 17–29. doi:10.1016/j.geomorph.2006.03.029
- Thomas, J. C., Cobbold, P. R., Shein, V. S., and Le Douaran, S. (1999). Sedimentary record of late paleozoic to recent tectonism in central Asia — Analysis of subsurface data from the turan and south kazak domains. *Tectonophysics* 313, 243–263. doi:10.1016/S0040-1951(99)00208-5
- Thomas, S. G. D. (1997). *Sand seas and aeolian bedforms. Arid zone geomorphology process, form and change in drylands*. John Wiley and Sons, 373–412.
- Tripaldi, A., Mehl, A., and Zárate, A. M. (2018). Parabolic megadunes in a subtropical Quaternary inland dune field, southwestern Pampas, Argentina. *Geomorphology* 321 (103–116), 103–116. doi:10.1016/j.geomorph.2018.08.021
- Tsoar, H. (2008). “Land use and its effect on the mobilization and stabilization of the NW Negev sand dunes,” in *Arid dune ecosystems*. Editors S. W. Breckle, A. Yair, and M. Veste (Berlin, Germany: Springer), 79–90. doi:10.1007/978-3-540-75498-5_6
- Tsoar, H. (2013). Critical environments: Sand dunes and climate change. *Treatise Geomorphol.* 11, 414–427. doi:10.1016/B978-0-12-374739-6.00314-6
- Tsoar, H. (2005). Sand dunes mobility and stability in relation to climate. *Phys. A Stat. Mech. its Appl.* 357, 50–56. doi:10.1016/j.physa.2005.05.067
- Twidale, C. R. (1981). Age and origin of longitudinal dunes in the Simpson and other sand ridge deserts. *Erde* 112, 231–241.
- Vandenbergh, J., Renssen, H., van Huissteden, K., Nugteren, G., Konert, M., Lu, H., et al. (2006). Penetration of atlantic westerly winds into central and East Asia. *Quat. Sci. Rev.* 25, 2380–2389. doi:10.1016/j.quascirev.2006.02.017
- Voigt, S., Weber, Y., Frisch, K., Bartenstein, A., Hellwig, A., Petschick, R., et al. (2017). Climatically forced moisture supply, sediment flux and pedogenesis in Miocene mudflat deposits of south-east Kazakhstan, Central Asia. *Depositional Rec.* 3, 209–232. doi:10.1002/dep2.34
- Walter, H., and Box, E. O. (1983). “The Karakum desert, an example of a well-studied eu-biome,” in *Ecosystems of the world; temperate deserts and semi deserts*. Editor N. E. West (Amsterdam, Netherlands: Elsevier), 105–159.
- Wang, X., Dong, Z., and Chen, Z. G. (2002). Geomorphology of sand dunes in the northeast taklimakan desert. *Geomorphology* 42 (3–4), 183–195. doi:10.1016/S0169-555X(01)00085-X
- Wasson, R. J., and Hyde, R. (1983). Factors determining desert dune type. *Nature* 304, 337–339. doi:10.1038/304337a0
- Wilson, I. G. (1973). *Ergs. Sediment. Geol.* 10, 77–106. doi:10.1016/0037-0738(73)90001-8
- Xu, X., Kleidon, A., Miller, L., Wang, S., Wang, L. Q., and Dong, G. (2010). Late quaternary glaciation in the tianshan and implications for palaeoclimatic change: A review. *Boreas* 39, 215–232. doi:10.1111/j.1502-3885.2009.00118.x
- Xu, Z., Mason, J. A., Xu, C., Yi, S., Bathiany, S., Yizhaq, H., et al. (2020). Critical transitions in Chinese dunes during the past 12,000 years. *Sci. Adv.* 6 (9), eaay8020. doi:10.1126/sciadv.aay8020
- Yizhaq, H., Ashkenazy, Y., and Tsoar, H. (2009). Sand dune dynamics and climate change: A modeling approach. *J. Geophys. Res.* 114, F01023. doi:10.1029/2008JF001138
- Zamani, S., Mahmoodabadi, M., Yazdanpanah, N., and Farpoor, H. F. (2020). Meteorological application of wind speed and direction linked to remote sensing images for the modeling of sand drift potential and dune morphology. *Meteorol. Appl.* 27, e1851. doi:10.1002/met.1851
- Zhenda, Z., and Youlin, Y. (1990). “The characteristics of sand dunes and its stabilization in China,” in *International workshop on sand transport and desertification in arid lands* (Singapore: World Scientific Publishing Co. Pte. Ltd.), 465–469. doi:10.1142/9789814541374
- Zhou, Y., Lu, H., Joseph, M., Miao, X., James, S., and Ronald, G. (2008). Optically stimulated luminescence dating of aeolian sand in the Otindag dune field and Holocene climate change. *Sci. China Ser. D Earth Sci.* 51, 837–847. doi:10.1007/s11430-008-0057-9

Nomenclature

KKCAD Karakum and Kyzylkum Central Asian deserts	CCKP Climate Change Knowledge Portal
OSL Optically stimulated luminescence	WBG World Bank Group
NOAA National Oceanic and Atmospheric Administration	CRU TS Climatic Research Unit gridded Time Series
DP Drift potential	UEA University of East Anglia
RDP Resultant drift potential	UDI Wind directionality index
VLDs Vegetated linear dunes	HSA Hot Spot Analysis
USSR Union of Soviet Socialist Republics	TSC Time-series partitioning around medoids (PAM) clustering
ECMWF European Center for Medium-Range Weather Forecasts	AOIs Areas of interest
4D-Var Four-dimensional variational data assimilation	RS Remote sensing
IFS Integrated forecast system	GIS Geographic information system
RDD Resultant drift direction	LGM Last glacial maximum